CrystEngComm

Cite this: *CrystEngComm*, 2011, **13**, 5788

www.rsc.org/crystengcomm

PAPER

Supramolecular architectures in *o*-carboranyl alcohols bearing *N*-aromatic rings: syntheses, crystal structures and melting points correlation†

Florencia Di Salvo,[a] Beatriz Camargo,[a] Yolanda García,[a] Francesc Teixidor,[a] Clara Viñas,[a] José Giner Planas,*[a] Mark E. Light[b] and Michael B. Hursthouse[b]

Received 15th April 2011, Accepted 14th June 2011
DOI: 10.1039/c1ce05449j

The syntheses of new *o*-carboranyl alcohols bearing *N*-aromatic rings, 1-[R(hydroxy)methyl]-2-methyl-1,2-dicarba-*closo*-dodecaborane (R = 6-methyl-2-pyridyl **1b**, 3-pyridyl **1c**, 2-quinolyl **1e**, 4-quinolyl **1f**), 1-[R(hydroxy)methyl]-1,2-dicarba-*closo*-dodecaborane (R = 2-pyridyl **2a**, 6-methyl-2-pyridyl **2b**, 3-pyridyl **2c**, 4-pyridyl **2d**, 2-quinolyl **2e**, 4-quinolyl **2f**)), are reported. The crystal structures of all compounds, except that for **1b**, are reported and compared with those related compounds previously synthesized by us (1-[R(hydroxy)methyl]-2-methyl-1,2-dicarba-*closo*-dodecaborane (R = 2-pyridyl **1a**, 4-pyridyl **1d**)). We provide an analysis of these compounds by means of X-ray crystallography, NMR/IR spectroscopies, thermal analyses and gas phase calculations in the context of crystal engineering. The results show that the crystal packings of these alcohols are dominated by the supramolecular O–H···N heterosynthon, but also include other weaker interactions such as C–H···O hydrogen bonds, H···H contacts and some degree of (C/B)–H···π interactions. There are four types of O–H···N hydrogen bonded chains, two giving rise to high melting point compounds (**1c**, **1d**, **1f**, **2c**, **2d**, and **2f**) and two affording lower melting point compounds (**1a**, **2a** and **2b**). The lowest melting compounds (**1e** and **2e**) show no such infinite O–H···N hydrogen bonding networks and only intramolecular O–H···N hydrogen bonds. We correlate the presence of the infinite O–H···N hydrogen bonding network in the crystal structure for the pyridine derivatives with their melting points. Gas phase calculations show that the energy for the O–H···N interactions in hydrogen bonded dimers is in the range 4–8 kcal mol^{-1}.

Introduction

Non-bonding intra- and intermolecular interactions are of fundamental importance for understanding molecular recognition phenomena, biological processes as well as physical and chemical properties of new materials.[1] The study of compounds containing boron continues to have an important impact on virtually every area of chemistry.[2] However, one of the few areas in which boron compounds have been neglected is crystal engineering.[3] We have recently related the field of molecular crystal engineering with that of icosahedral heteroborane clusters.[4] The latter comprise carbon containing polyhedral boranes—*carboranes* (Chart 1)—and their metal complexes—*metallacarboranes*. Our interest in these boron based molecular materials is triggered by their properties, such as high thermal and chemical stability, hydrophobicity, their acceptor character and the possibility to introduce transition metals in the clusters to form metallacarboranes.[5] The three-dimensional nature of the icosahedral heteroborane clusters makes these molecules valuable building blocks in supramolecular systems.[6] Carborane supramolecular chemistry is mainly directed by their acidic C*c*–H (C*c* = cage carbon) vertices as proton donors of type C*c*–H···X with classical (X = O, N, S, F, Cl, Br, I)[5,7] and weak non-classical (X = alkynes, arenes)[5,8] proton acceptors. Heteroborane clusters also

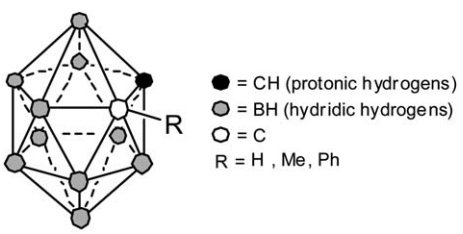

closo-[2-R-1,2-$C_2B_{10}H_{12}$]

Chart 1 *ortho*-Carbonate molecules.

[a]*Institut de Ciència de Materials de Barcelona (ICMAB-CSIC), Campus U.A.B., 08193 Bellaterra, Spain. E-mail: jginerplanas@icmab.es; Fax: +34 93 580 57 29; Tel: +34 93 188 87 86*
[b]*School of Chemistry, University of Southampton, Highfield, Southampton, UK SO17 1BJ; Fax: +44 (0)2380596723; Tel: +44 (0)2380596721*

† Electronic supplementary information (ESI) available: IR spectra and DTA for all compounds, melting point plots, computational details and Hirshfeld surface analyses. CCDC reference numbers 816754 (**1c**), 816755 (**1e**), 816756 (**1f**), 816749 (**2a**), 816757 (**2b**), 816751 (**2c**), 816750 (**2d**), 816752 (**2e**), 816753 (**2f**). For ESI and crystallographic data in CIF or other electronic format see DOI: 10.1039/c1ce05449j

form nonconventional hydrogen bonds such as dihydrogen bonds, involving H centers as both the donor and acceptor of the type D–H···H–B (D = C, O, N, S).[4b,9]

We have previously synthesized a series of *o*-carboranyl alcohols (Scheme 1) and determined their crystal structures.[4f] We found that O–H···O homosynthons are formed in the less bulkier alcohols having *C*,*O*-aromatic rings (bottom of Scheme 1), all of them forming hydrogen bonded tetramers. The latter are avoided as the carboranyl alcohols become bulkier (*steric control*) and give rise to weaker intermolecular O–H···π hydrogen bonds and/or π–π interactions. We anticipated that in those alcohols having an additional hydrogen bond acceptor such as a nitrogen atom (**1a** and **1d**, Scheme 1), the interplay of competing hydrogen bond interactions (O–H···O *versus* O–H···N) will control the molecular organization in the crystal lattice to yield various supramolecular architectures. In fact, the inclusion of an aromatic nitrogen in these molecules shifted the supramolecular situation to the more stable O–H···N heterosynthon giving centrosymmetric dimers for **1a** through bifurcated O–H···$(N)_2$ hydrogen bonds, one intra- and one intermolecular but an infinite O–H···N hydrogen bonding network in the crystal structure for compound **1d**.

In our earlier work, we posed the question of whether this supramolecular heterosynthon would be robust enough and reproducible in order to create new solid state structures.[4f] In the present paper, we describe the synthesis and characterization of ten new nitrogenated aromatic N_{AR} carboranyl alcohols (Scheme 2) and supramolecular characterization of nine of them, as a part of our interest in molecular crystal engineering of icosahedral heteroborane clusters and of our wider strategy aimed at providing new organic–inorganic hybrid functional molecular materials.[10] An investigation of close intermolecular contacts of the new molecules and those for previously reported **1a** and **1d** *via* Hirshfeld surface analysis is also presented in order to reveal the subtle differences and similarities of the N_{AR} carboranyl alcohols in the eleven crystal structures. We attempt to find the correspondence between molecular structure and crystal structure and the relation between the supramolecular structures and melting points/thermal behaviour of these compounds.

Results and discussion

The new alcohols derived from the methyl-*o*-carborane (**1b,c** and **e,f**) have been prepared as previously described[4f,11] by the reaction of lithiated methyl-*o*-carborane clusters with different aromatic aldehydes at low temperature and isolated in good yields (45–78%). However, the preparation of the related *o*-carborane derivatives is not trivial because the monolithiation of the *o*-carborane moiety is complicated by the tendency of the monolithio *o*-carborane to disproportionate to *o*-carborane and its dianion.[12] Several strategies have been followed to overcome this problem, such as for example by using protecting/deprotecting methodologies, using dimethoxyethane as the solvent or by doing the reaction at high dilution.[13] We have recently gained experience in our group on such a monolithiation and the further reaction with various electrophiles and found that it can be easily done in ethereal solvents at very low temperature (<−70 °C).[14] Following this strategy, we have been able to prepare exclusively the monosubstituted alcohols derived from the *o*-carborane (**2a–f**) in good to excellent yields (62–88%), by carrying out the reaction in diethyl ether instead of THF and keeping the temperature low in all steps of the reaction (Scheme 3 and Experimental section). All new compounds have been fully characterized by ^{1}H, $^{1}H\{^{11}B\}$, ^{11}B, $^{11}B\{^{1}H\}$ and $^{13}C\{^{1}H\}$ NMR spectroscopy and the data correlated well with those of related alcohols.[4f,11f] Table 1 summarizes selected spectroscopic data for the present and previously synthesized alcohols. $^{11}B\{^{1}H\}$ NMR spectra for all compounds are consistent with a *closo*-icosahedral geometry for the boron cage.[15] $^{13}C\{^{1}H\}$ NMR spectra also show characteristic peaks for the two cage-carbon vertices, N_{AR} rings and benzyl *C*H carbons. Compounds **2a–f** show a broad resonance for the C*cH* (C*c* = cage carbon) proton at δ 4.41–4.97, in agreement with the monosubstitution of the cage. Proton resonances for the O*H* and C*H*OH groups in the new compounds appeared in the same range as that for the previously reported alcohols **1a** and **1d** and have now been unambiguously confirmed for **2a** by ^{1}H-$^{13}C\{^{1}H\}$ heterocosy.[11a,4f] Signals for the O*H* and C*H*OH groups in these compounds appear as two doublets of *ca.* 5–7 Hz in most cases. The high chemical shift for the OH signal in all alcohols and concentration independence in alcohols **1a** and **1d**[11a] are explained by a solution persistent intra- and/or intermolecular O–H···N hydrogen bond.

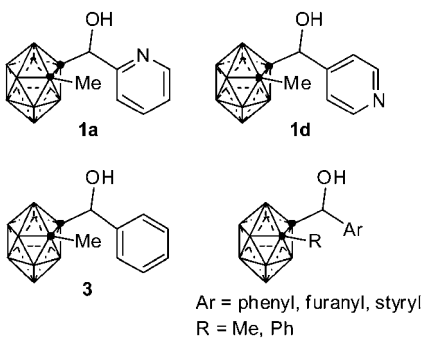

Scheme 1 Previously characterised carboranyl alcohols.[4f]

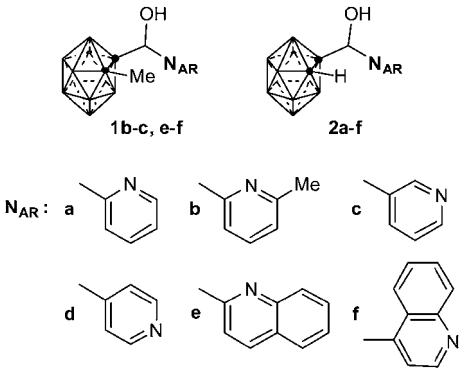

Scheme 2 New compounds.

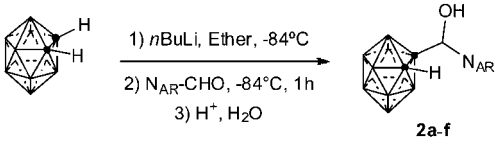

Scheme 3

Table 1 Chemical structures, selected spectroscopic data, infrared O–H stretching bands (ν_{OH})[a] and melting points (mp)[b] for the compounds studied

Compound number	Chemical structure	δ O*H*	δ C*H*OH	ν_{OH}/cm^{-1}	3394[c] ν_{OH}/cm^{-1}	Mp/°C
1a[d]	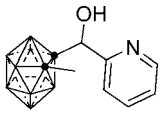	5.86	5.35	3356 s, vbr	38	137
1b	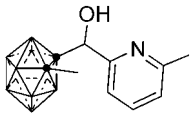	5.78	5.29	3141 s, vbr	253	107
1c	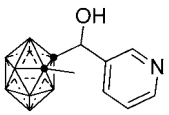	6.02	5.49	3080 s, vbr	314	220
1d[d]	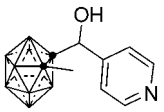	6.05	5.43	3089 s, vbr	305	256
1e	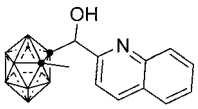	6.17	5.55	3394[c] s, br	0	130
1f	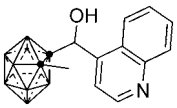	6.30	6.17	3043 s, vbr	351	—[ef]
2a	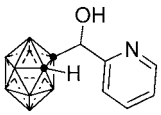	5.96	5.36	3074[g] s, vbr	320	154
2b	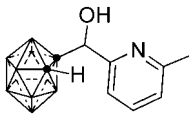	5.90	5.30	3037[g] s, vbr	357	154
2c	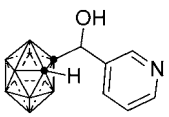	6.29	5.51	3050[g] s, vbr	344	211
2d	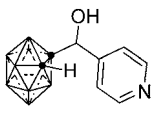	6.37	5.45	3062[g] s, br	332	248
2e	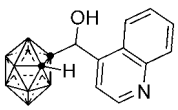	6.25	5.55	3337 s, br	57	121
2f	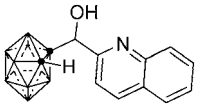	6.53	6.32	3031[g] s, vbr	363	—[eh]

[a] In KBr. Nomenclature: s (strong), br (broad), sh (sharp), v (very). [b] Melting points measured by DSC or DTA unless noticed. Compounds **1a** and **1b** melt but all others melt with decomposition. [c] Frequency for the highest O–H stretching band found in this table (compound **1e**). [d] ref. 4*f*. [e] Thermal behaviour examined by hot-stage microscopy (HSM). [f] Sublime without melting. [g] Estimated value due to overlapped bands. [h] Decomposed without melting.

Solid state IR spectra for all compounds show diagnostic signals for the OH and BH stretching frequencies in the ranges 3394–3031 and 2630–2561 cm^{-1}, respectively. IR frequencies for the OH bands (Table 1) are very informative on the presence and strength of hydrogen bonding structures. Analysis of the OH bands for our compounds clearly shows two distinct and clear

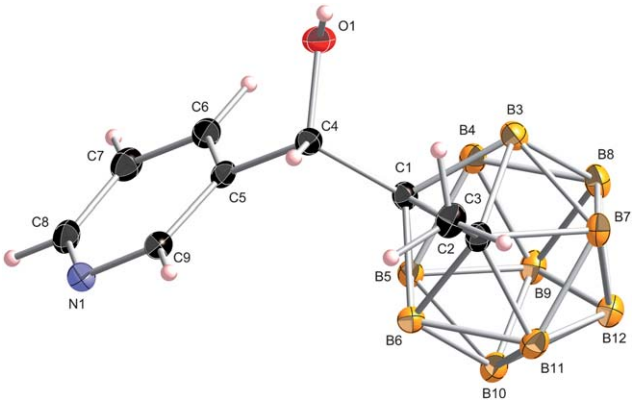

Fig. 1 Molecular structure of **1c**; thermal ellipsoids set at 35% probability (B–H, pyridine and methyl hydrogen atoms are omitted for clarity). Selected interatomic distances (Å) and angles (°): C1–C2 1.680(3), C1–C4 1.564(3), C4–C5 1.518(3), C4–O1 1.401(2), C1C4O1 111.23(15), C1C4C5 111.06(15).

situations: whereas compounds **1a**, **1e** and **2e** show sharp or broad bands at high stretching frequencies (3394–3337 cm^{-1}), the rest of the compounds in Table 1 show red shifted (3141–3031 cm^{-1}) and very broad bands which is a clear indication of hydrogen bonding.[1] The latter can be clearly seen when subtracting the stretching frequencies of the alcohols from the one with the highest frequency OH sharp resonance (**1e**, fifth column in Table 1) that we take as the reference.

Melting points for our compounds were measured by Differential Scanning Calorimetry (DSC) or Differential Thermal Analysis (DTA) and showed that whereas compounds **1a** and **1b** clearly melted at 137 and 107 °C, respectively, all other compounds melt with decomposition in the range 121–256 °C (Table 1).

Molecular structures

The molecular structures for compounds **1c**, **1e,f** and **2a–f** have been unequivocally established by X-ray crystallography (Fig. 1–9) and are in agreement with the NMR data. Crystal and data collection details can be found in Table 2 and Experimental section. Whereas racemic **1c**, **1e,f**, **2a–d** and **2f** crystallize in centrosymmetric space groups (Table 2), compound **2e** crystallizes in the noncentrosymmetric space group $P2_1$. The molecular structures of all these alcohols show typical icosahedrons with very similar bond distances and angles, and also similar to those in other *o*-carboranyl alcohols.[4f,11] Carbon–oxygen bond lengths (Fig. 1–9) are consistent with a single C–O bond. The pivotal role hydrogen bonding plays in the supramolecular architecture makes the accurate location of the OH hydrogen position critical. In all cases the position of the hydrogen atom was clear from examination of the difference map. In **1c**, **1e**, **1f**, **2b** it was possible to refine the hydrogen freely without any geometrical or thermal parameter restraints, for **2c**, **2d**, **2e** and **2f** it was necessary to apply O–H distance restraints (0.84 Å) and thermal parameter restraints (1.5 that of the parent oxygen), however the final position of the hydrogen always matched very closely the location of the initial peak observed in the difference map. The situation for **2a** is complicated by a disorder involving the location of the OH group. In the major component (*ca.* 86%) the OH hydrogen is hydrogen bonded to a nitrogen atom of a contiguous

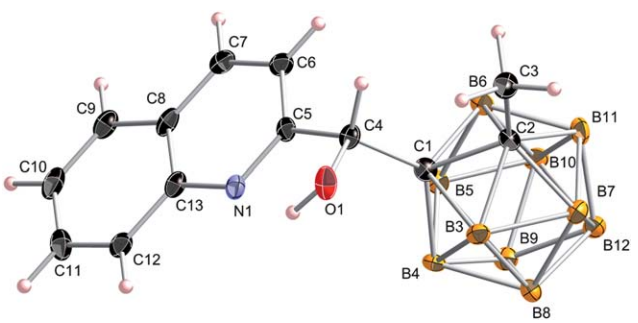

Fig. 2 Molecular structure of **1e**; thermal ellipsoids set at 35% probability (All hydrogen atoms, except that for the OH, are omitted for clarity). Selected interatomic distances (Å) and angles (°): C1–C2 1.684 (5), C1–C4 1.553(5), C4–C5 1.517(5), C4–O1 1.400(4), C1C4O1 110.8(3), C1C4C5 110.8(3).

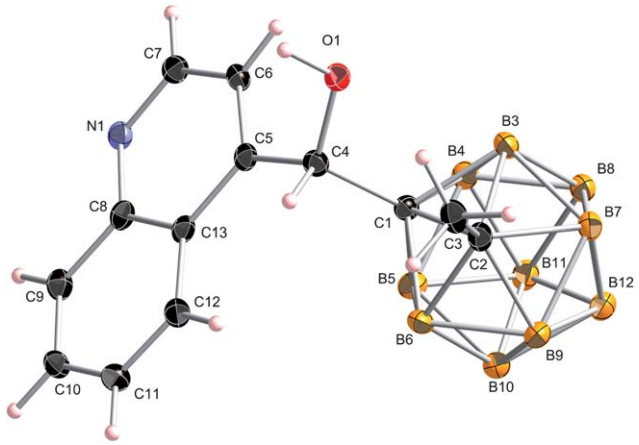

Fig. 3 Molecular structure of **1f**; thermal ellipsoids set at 35% probability (B–H, quinolyl and methyl hydrogen atoms are omitted for clarity). Selected interatomic distances (Å) and angles (°): C1–C2 1.681(3), C1–C4 1.552(3), C4–C5 1.529(3), C4–O1 1.404(3), C1C4O1 107.48(17), C1C4C5 112.55(17).

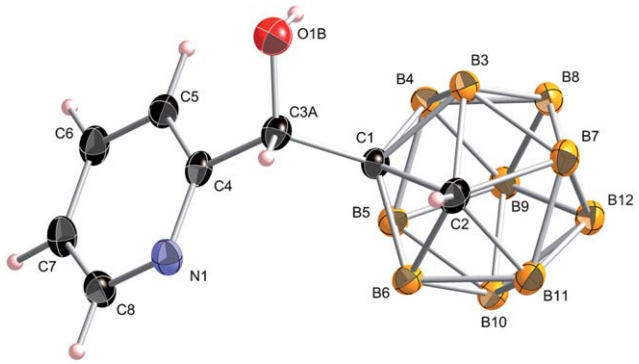

Fig. 4 Molecular structure of **2a**; thermal ellipsoids set at 35% probability (disorder and B–H hydrogen atoms are omitted for clarity). Selected interatomic distances (Å) and angles (°): C1–C2 1.660(2), C1–C3A 1.551(2), C3A–C4 1.513(3), C3A–O1 1.423(2), C1C3AO1 109.75 (15), C1C3AC4 111.61(15).

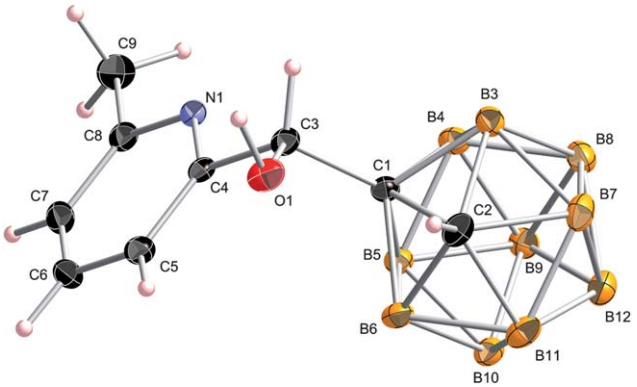

Fig. 5 Molecular structure of **2b**; thermal ellipsoids set at 35% probability (B–H and pyridine hydrogen atoms are omitted for clarity). Selected interatomic distances (Å) and angles (°): C1–C2 1.640(2), C1–C3 1.556(2), C3–C4 1.520(2), C3–O1 1.3990(19), C1C3O1 107.46(13), C1C3C4 110.66(12).

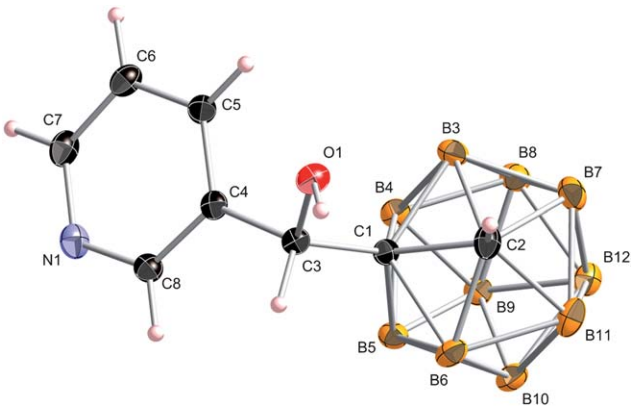

Fig. 6 Molecular structure of **2c**; thermal ellipsoids set at 35% probability. Selected interatomic distances (Å) and angles (°): C1–C2 1.635(2), C1–C3 1.560(2), C3–C4 1.511(2), C3–O1 1.403(2), C1C3O1 110.61(13), C1C3C4 110.54(13).

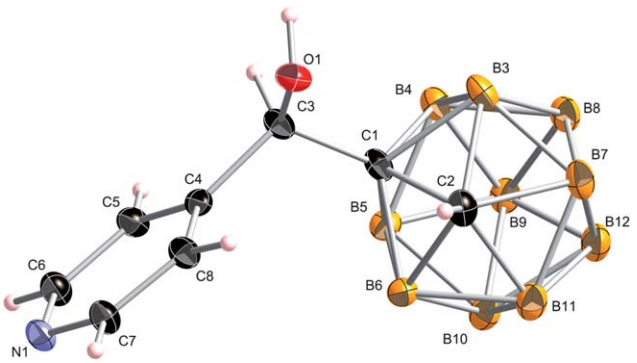

Fig. 7 Molecular structure of **2d**; thermal ellipsoids set at 35% probability. Selected interatomic distances (Å) and angles (°): C1–C2 1.642(5), C1–C3 1.557(5), C3–C4 1.518(4), C3–O1 1.394(4), C1C3O1 111.1(3), C1C3C4 113.6(3).

molecule whilst in the minor component no hydrogen bond is formed. In this case no suitable peaks were observed in the difference map and the hydrogen atoms were located in an idealised position with the torsion angle refined against the highest residual density. The comparison of the supramolecular structures with all other molecules in this work and, more importantly, the IR stretching band for the OH in compound **2a** (Table 1) are clear indications that the position of the OH hydrogen in this compound is that where it is hydrogen bonded.

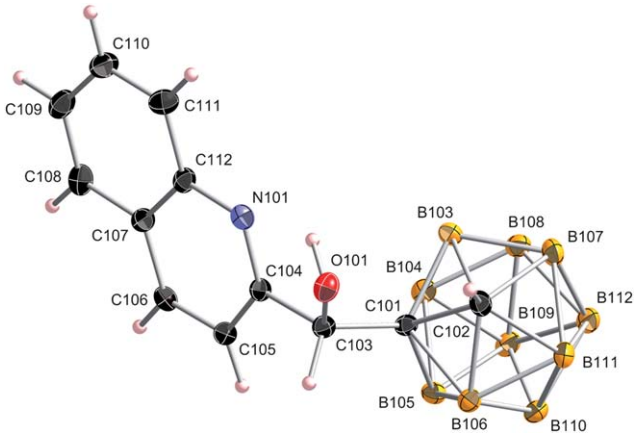

Fig. 8 Molecular structure of **2e**; thermal ellipsoids set at 35% probability, the first of 2 independent molecules in the asymmetric unit shown. Selected interatomic distances (Å) and angles (°): C101–C102 1.647(5), C101–C103 1.548(5), C103–C104 1.532(5), C103–O101 1.405(5), C101C103O101 110.1(3), C101C103C104 111.5(3).

Supramolecular structures

For convenience, we have normalised all crystal structures in the present study to the neutron distances.[1] This has little effect on strong or moderate hydrogen bonds but it is relevant when looking at very weak hydrogen or dihydrogen bonds.[1,4] For this reason, we will describe in detail the supramolecular structures of **1a** and **1d** again[4f] and compare them with all new compounds in this report. Crystal structures of all alcohols in this study are based on hydrogen bonds involving the OH groups and the nitrogen of the aromatic rings exclusively (Fig. 10–12 and Table 3). The distances of all of the observed intra- and/or intermolecular O–H···N hydrogen bonds are substantially shorter than the 2.75 Å distance that corresponds to the sum of the van der Waals radii ($\sum$vdW) of hydrogen and nitrogen atoms (Table 3) and those intermolecular ones are near-linear. Thus, they qualify as moderate hydrogen bonds.[1] Even though the packing is essentially governed by strong O–H···N hydrogen bonds in most cases, the structures also show a high number of other short contacts as listed in Table 4. In order to better understand the supramolecular structures of these molecules, we will divide the compounds into two groups; *Group A*: those whose N atom of the aromatic ring is *close* to the OH group (2-pyridyl, 6-Me-2-pyridyl and 2-quinolyl; see Scheme 2 and Fig. 10 and 11) and *Group B*: those having the N atom *farther away* from the OH groups (3- and 4-derivatives of pyridyl and quinolyl; see Scheme 2 and Fig. 12). In addition, we will compare those pairs of related Me-*o*-carboranyl and *o*-carboranyl structures whenever available in order to investigate the effect of C*c*-substitution of the carborane cage.

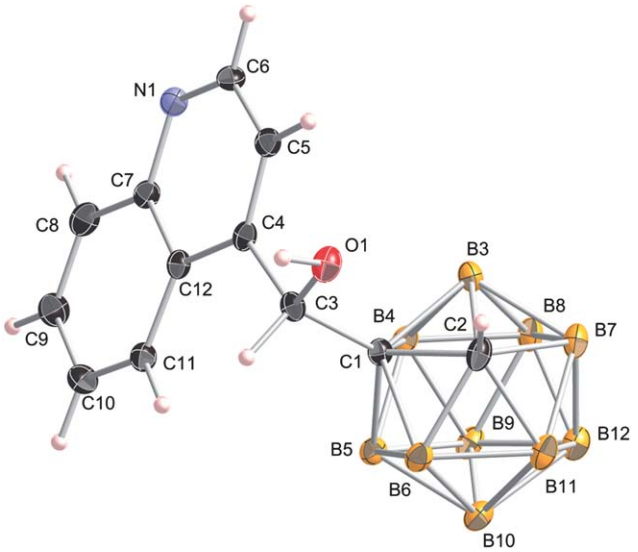

Fig. 9 Molecular structure of **2f**; thermal ellipsoids set at 35% probability. Selected interatomic distances (Å) and angles (°): C1–C2 1.658(3), C1–C3 1.559(3), C3–C4 1.529(3), C3–O1 1.392(2), C1C3O1 106.00(15), C1C3C4 110.61(15).

Group A: 2-substituted *N*-aromatic rings. As previously described,[4f] alcohol **1a** (having the *o*-carboranyl and 2-pyridyl fragments) forms centrosymmetric dimers through bifurcated O–H···$(N)_2$ hydrogen bonds, one intra- and one intermolecular along a similar direction to that of the *b* axis (Fig. 10, top, and Table 3). In addition, the dimers are closely packed by intermolecular $(C–H)_2$···O interactions and C–H···H–B contacts giving the polymeric network shown in Fig. 10 (upper pictures) and Table 4. On the other hand, alcohol **2a** (having the Me-*o*-carboranyl and 2-pyridyl fragments) forms chains in the solid state in which the molecules are linked exclusively by intermolecular O–H···N and C–H···O interactions parallel to the *b* axis (Fig. 10, middle). The crystal structure of **2b**, where the bulkiness around the N atoms is significantly increased due to the presence of a methyl group in position 6 of the pyridine, also features a similar supramolecular situation to that observed in the case of alcohol **2a**. As shown in Fig. 10 (bottom), alcohol **2b** forms hydrogen bonded chains based on intermolecular O–H···N interactions and C–H···H–B contacts (Tables 3 and 4).

The solid structures of **1a**, **2a** and **2b** consist of three-dimensional (3D) structures built by self-assembly of the polymeric hydrogen bonded networks shown in Fig. 10, which are dominated by weak dihydrogen and/or hydrophobic interactions.

Crystal structures of the 2-quinolyl derivatives **1e** and **2e** show a different supramolecular situation to that of the related 2-pyridyl derivatives since only intramolecular O–H···N hydrogen bonds are found in both cases (Fig. 11). In addition, a variety of weak intermolecular interactions (C–H···O, C–H···π and C–H···H–B) are found for this compound as summarized in Table 4.

Group B: 3 and 4-substituted *N*-aromatic rings. For geometric reasons, the formation of intramolecular O–H···N hydrogen bonds is not possible in those alcohols containing 3- and 4-pyridyl or 4-quinolyl fragments (**1** and **2c**, **2d** and **2f**; Scheme 2 and Fig. 12). Therefore, crystal structures of the Me-*o*-carboranyl based alcohols **1c**, **1d**, **1f** and their related *o*-carboranyl alcohols **2c**, **2d** and **2f** show all supramolecular 1D chains sustained on intermolecular O–H···N hydrogen bonds (Fig. 12 and Scheme 4). Table 3 lists the salient intermolecular distances and angles. The angles α between the oxygen atoms of three consecutive molecules have been used as descriptors for this type of supramolecular chain arrangements.[16] The latter values represent the chain folding that can be visualized in Fig. 12. Interestingly, whereas in both 3-pyridyl derivatives (**1c** and **2c**), the carboranyl cages of the hydrogen bonded molecules in the chain are all in the same side with respect to the hydrogen bonding network, in those for the 4-substituted-*N*-aromatic derivatives (**1d**, **2d**, **1f** and **2f**) the carboranyl cages alternate over and below the network as shown in Fig. 12. Another interesting feature is that all O–H···N chains, except those for **1d** and **1f**, are formed by alternating *R* and *S* enantiomers. Thus, each supramolecular chain in the solid structures for **1d** and **1f** is formed by only one of the two possible enantiomers.

The crystal structures in compounds **1c** and **2c** reveal a very similar packing of molecules and can thus be regarded as isomorphous. The packings of these two compounds consist of two-dimensional (2D) structures where the hydrogen bonded 1D chains associate by weak C–H···O hydrogen bonds giving the wave-like layered structure shown in Fig. 13. The 3D structures for these compounds are then formed by association of the wave-like 2D structures through short B–H···π contacts as shown in Fig. 13.[17]

On the other hand, although the O–H···N hydrogen bonded 1D chains in **1d** and **2d** are very similar, their packings show some differences. Fig. 14 shows a comparison of the assembly of 1D chains in both compounds. At first look, both 2D structures resemble each other. However there are significant differences. As already mentioned above, while the supramolecular chains in **1d** are formed by only one of the two possible enantiomers, those of the related compound **2d** are composed of both alternating enantiomers. Thus, the normal-coloured chain for **1d** in Fig. 14 is composed of *R* isomers whereas the yellow one is made of *S* enantiomers exclusively. In the case of **2d** all chains are made of *RSRS*… enantiomers. Another important difference between the solid structures of these compounds is that in compound **1d**, the enantiomerically pure 1D chains are interacting by very weak C–H···H–B contacts (Fig. 14 and Table 4) but the racemic 1D chains in **2d** interact through stronger bifurcated C–H···O hydrogen bonds. The 3D structure in both **1d** and **2d** is then formed by the assembly of OHN hydrogen bonding chains.

Interestingly, compound **1f** forms enantiopure O–H···N hydrogen bonded 1D chains as already observed for its pyridyl analogue **1d**. On the other hand, **2f** forms racemic 1D chains as shown in Fig. 12. A first look to Fig. 12 and the α values (Table 1) shows a clear contraction of the OHN chains in the case of 4-quinolyl derivatives, **1f** (α = 85°) and **2f** (α = 121°). The contraction of the supramolecular OHN chains in these two compounds can be explained by the existence of intermolecular π–π interactions between the quinolyl rings of chains in both cases (interplanar and centroid–centroid distances in Å): 3.279 and 3.740 (**1f**), 3.386 and 4.237 (**2f**), respectively. A comparison of the supramolecular structures shown in Fig. 15 evidences that in compound **1f** π–π stacking occurs between alternate quinolyl

Table 2 Crystallographic parameters for compounds **1c**, **1e**, **1f**, and **2a–f**[a]

	1c	**1e**	**1f**	**2a**	**2b**	**2c**	**2d**	**2e**	**2f**
Empirical formula	$C_9H_{19}B_{10}NO$	$C_{13}H_{21}B_{10}NO$	$C_{13}H_{21}B_{10}NO$	$C_8H_{17}B_{10}NO$	$C_9H_{19}B_{10}NO$	$C_8H_{17}B_{10}NO$	$C_8H_{17}B_{10}NO$	$C_{12}H_{19}B_{10}NO$	$C_{12}H_{19}B_{10}NO$
Formula weight	265.35	315.41	315.41	251.33	265.35	251.33	251.33	301.38	301.38
Crystal system	Monoclinic	Monoclinic	Orthorhombic	Monoclinic	Monoclinic	Monoclinic	Monoclinic	Monoclinic	Monoclinic
Space group	$P2_1/n$	$P2_1/n$	$Pbca$	$P2_1/c$	$C2/c$	$P2_1/n$	$P2_1/n$	$P2_1$	$C2/c$
a/Å	9.8268(2)	11.6364(16)	10.4622(2)	10.4340(3)	21.1947(7)	9.7297(2)	13.0921(3)	7.2182(2)	25.8502(4)
b/Å	13.4445(4)	11.4228(16)	10.4196(3)	6.7029(2)	7.1376(2)	12.8208(2)	8.7487(2)	19.7365(4)	9.7968(2)
c/Å	11.3957(3)	13.1428(14)	30.6975(9)	20.4814(6)	19.7547(6)	11.5304(2)	13.6578(4)	11.3467(3)	12.8393(2)
β/o	105.640(2)	105.666(12)	—	103.747(2)	92.129(2)	104.9020(10)	118.2650(10)	90.4040(10)	96.4100(10)
Volume/Å^3	1449.81(6)	1682.0(4)	3346.39(15)	1391.40(7)	2986.41(16)	1389.96(4)	1377.83(6)	91 616.43(7)	3231.22(10)
Z	4	4	8	4	8	4	4	4 (2 molec.)	8
ρ_{calcd}/g cm^{-3}	1.216	1.245	1.252	1.200	1.180	1.201	1.212	1.238	1.239
Absorption coefficient/mm^{-1}	0.064	0.067	0.067	0.063	0.063	0.064	0.064	0.066	0.066
F(000)	552	656	1312	520	1104	520	520	624	1248
Crystal	Fragment; colourless	Fragment; colourless	Fragment; colourless	Block; colourless	Block; colourless	Fragment; colourless	Fragment; colourless	Block; colourless	Fragment; colourless
Crystal size/mm	0.2 × 0.13 × 0.06	0.3 × 0.18 × 0.10	0.32 × 0.22 × 0.07	0.3 × 0.2 × 0.15	0.35 × 0.3 × 0.1	0.2 × 0.12 × 0.07	0.09 × 0.07 × 0.02	0.29 × 0.1 × 0.07	0.22 × 0.2 × 0.18
θ range for data Collection/°	3.20–27.48	3.22–25.03	3.06–27.48	3.21–27.48	3.01–27.48	2.92–27.48	2.92–25.03	3.00–27.48	3.16–25.03
Reflections collected	15 492	2964	30 061	18 069	23 120	15 768	30 667	15 597	15 346
Independent reflections	3301 [$R_{int} = 0.0514$]	2964 [$R_{int} = 0.0000$]	3834 [$R_{int} = 0.1179$]	3187 [$R_{int} = 0.0576$]	3424 [$R_{int} = 0.0679$]	3181 [$R_{int} = 0.0414$]	2444 [$R_{int} = 0.1157$]	3793 [$R_{int} = 0.0548$]	2848 [$R_{int} = 0.0463$]
Completeness to $\theta = 27.48°$	99.4%	99.7%	99.9%	99.7%	99.8%	99.5%	99.9%	99.3%	99.7%
Max. and min. transmission	0.9961 and 0.9872	0.9934 and 0.9802	0.9953 and 0.9788	0.9905 and 0.9812	0.9938 and 0.9784	0.9956 and 0.9874	0.9987 and 0.9943	0.9954 and 0.9869	0.9882 and 0.9855
Largest difference peak and hole/ e Å^{-3}	0.315 and −0.245	0.328 and −0.746	0.376 and −0.411	0.637 and −0.381	0.582 and −0.400	0.349 and −0.281	0.667 and −0.233	0.235 and −0.230	0.423 and −0.327
Data/restraints/ parameters	3301/0/195	2964/0/231	3834/0/230	3187/0/188	3424/0/195	3181/0/182	2444/0/182	3793/1/436	2848/0/218
Goodness-of-fit on F^2	1.057	1.063	1.048	1.062	1.062	1.063	1.099	1.157	0.998
Final R indices [$F^2 > 2\sigma(F^2)$]	$R1 = 0.0640$, $wR2 = 0.1541$	$R1 = 0.0989$, $wR2 = 0.2428$	$R1 = 0.0660$, $wR2 = 0.1585$	$R1 = 0.0645$, $wR2 = 0.1711$	$R1 = 0.0583$, $wR2 = 0.1584$	$R1 = 0.0596$, $wR2 = 0.1398$	$R1 = 0.0863$, $wR2 = 0.1776$	$R1 = 0.0540$, $wR2 = 0.1172$	$R1 = 0.0553$, $wR2 = 0.1406$
R indices (all data)	$R1 = 0.0880$, $wR2 = 0.1729$	$R1 = 0.1483$, $wR2 = 0.2752$	$R1 = 0.1111$, $wR2 = 0.1813$	$R1 = 0.0873$, $wR2 = 0.1862$	$R1 = 0.0774$, $wR2 = 0.1715$	$R1 = 0.0718$, $wR2 = 0.1476$	$R1 = 0.1128$, $wR2 = 0.1924$	$R1 = 0.0619$, $wR2 = 0.1231$	$R1 = 0.0669$, $wR2 = 0.1516$

[a] CCDC 816754 (**1c**), 816755 (**1e**), 816756 (**1f**), 816749 (**2a**), 816757 (**2b**), 816751 (**2c**), 816750 (**2d**), 816752 (**2e**), 816753 (**2f**).

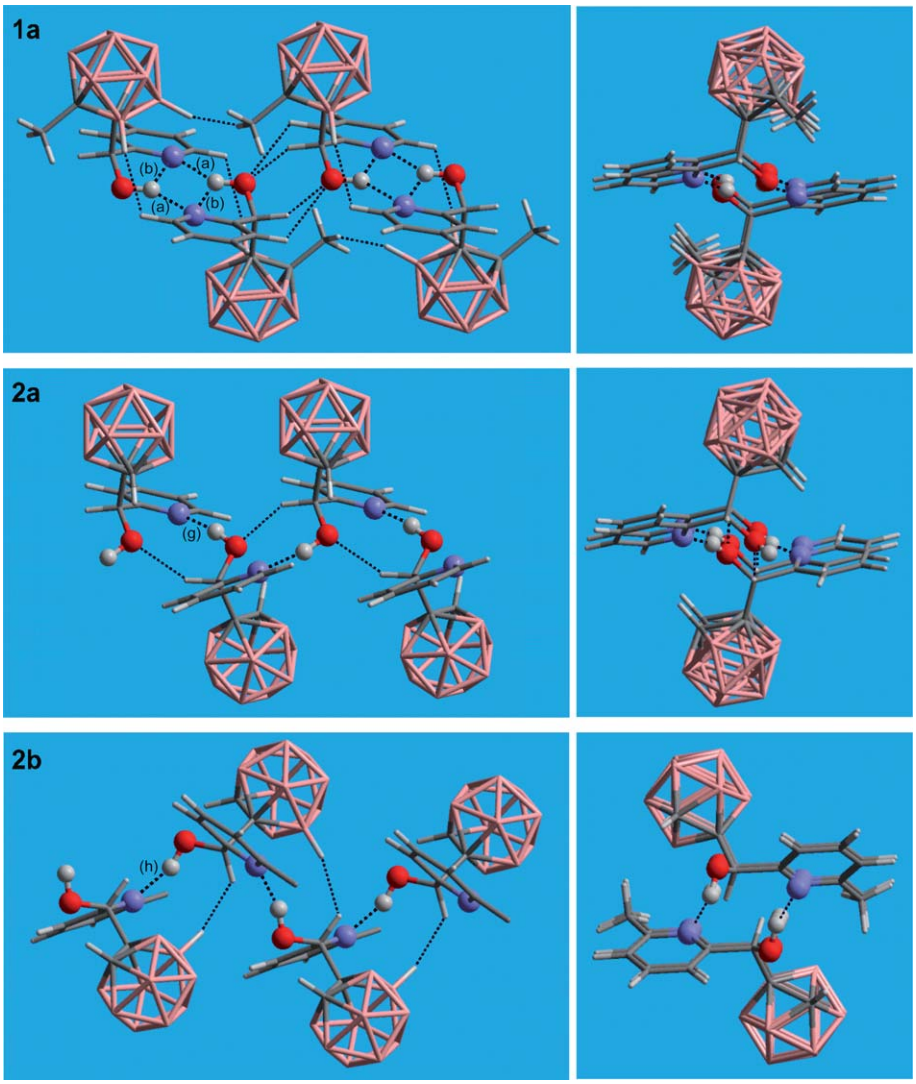

Fig. 10 Supramolecular assemblies of **1a**, **2a** and **2b** in the type I–II structures (Scheme 4). Left column: projections showing 4 molecules of each compound forming hydrogen bonded layers. Right column: projections along the hydrogen bonded layers. See Tables 3 and 4 for metric parameters. All hydrogen atoms, except those hydrogen bonded, are omitted for clarity. Color code: B pink; C grey; H white; O red; N blue.

rings of different 1D chains. Assembly of the "available" quinolyl rings in Fig. 15 with another chain (not shown in the figure) by π–π interactions gives rise to the 3D structure of **1f**. In contrast, the supramolecular structure **2f** shows that all quinolyl rings of different 1D chains interact by π–π stacking giving the 2D structure shown in Fig. 15. The close packing of the 2D structure forms the 3D one for these compounds.

Hirshfeld surface generation and fingerprint plot analysis

The Hirshfeld surface analysis is a valuable method for the analysis of intermolecular contacts that offer a whole-of-the-molecule approach.[18] Thus, a Hirshfeld surface analysis has been performed for all compounds in this study, producing a 2D-fingerprint plot for each (Fig. 16). The fingerprint plots fully agree with the supramolecular structures described above and confirm that these compounds share some similar supramolecular features: O–H···N (labelled A) and C–H···O (labelled B) hydrogen bonds, H···H contacts (C) and some degree of (C/B)–H···π interactions (D). The O–H···N intermolecular interactions appear as two distinct spikes (A) that are present in all compounds except **1e** and **2e** (Fig. 16). This is consistent with the OH stretching frequencies in their IR spectra (Table 1). The C–H···O spikes (B) are only visible in compounds **1a**, **2a** and **2d**. The intermolecular H···H contacts in the limit of the van der Waals radii appear as a characteristic hump (C) in the central region of all compounds.

The relative contribution of different interactions to the Hirshfeld surface was calculated. Decomposed fingerprint plots are presented in the ESI†. This decomposition enables separation of contributions from different interaction types, which commonly overlap in the full fingerprint. It also facilitates rapid comparison between related molecules in the same or different crystals.[18c,e] As part of this decomposition analysis, the fraction of the Hirshfeld surface representing a given interaction was calculated (Fig. 17). From this simple analysis, it immediately

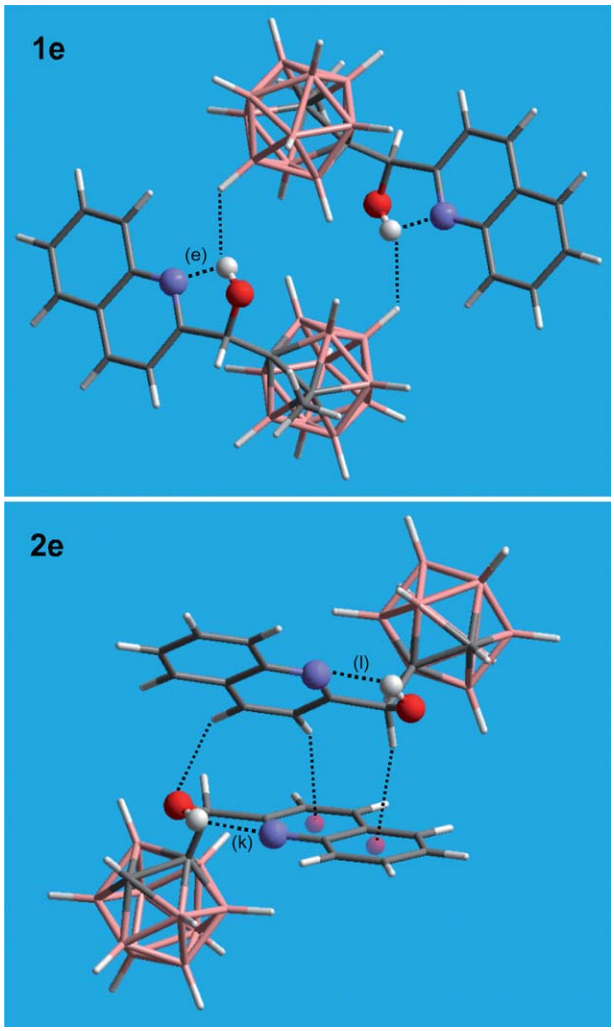

Fig. 11 Supramolecular assemblies of **1e** and **2e**. Projection showing 2 molecules of the compounds, showing all intra- and intermolecular contacts. See Tables 3 and 4 for metric parameters. Color code: B pink; C grey; H white; O red; N blue.

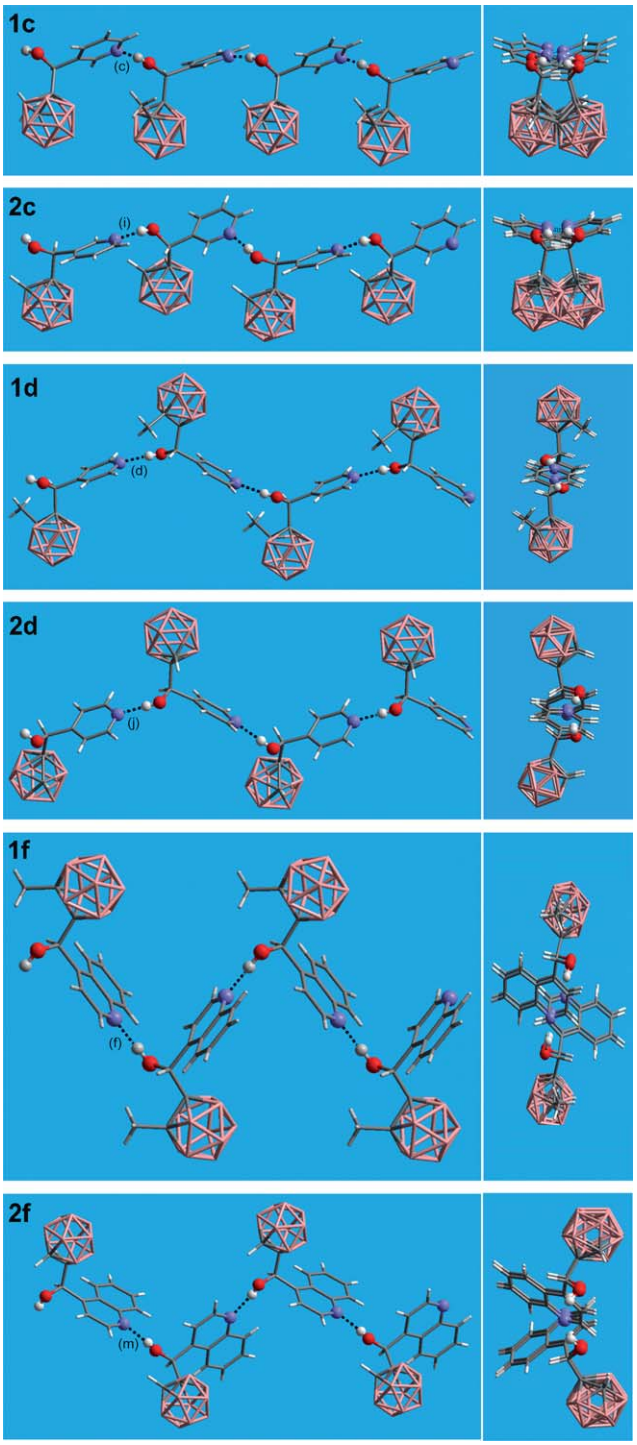

Fig. 12 Supramolecular assemblies of **1c,d**, **1f**, **2c,d** and **2f** in the type III–IV structures (Scheme 4). Left column: supramolecular assemblies showing infinite hydrogen bonding networks. Right column: projections along the hydrogen bonded networks. See Table 3 for metric parameters. All BH hydrogen atoms are omitted for clarity. Color code: B pink; C grey; H white; O red; N blue.

emerges that H···H contacts comprise nearly 80% of the total Hirshfeld surface area for these molecules. This is not surprising taking into account the large ratio of external H to N, O or C atoms in each molecule due to the carborane cages. C···H (*i.e.* C/B–H···π) contacts contribute around 10% to the total Hirshfeld surface area for **1a–d**, **1f**, **2a–d** and **2f** and 20% for **1e** and **2e**. The contribution of H···N (*i.e.* O–H···N) and H···O (*i.e.* C–H···O) interactions varies from 2 to 9% and 2 to 6%, respectively. Finally, a small percentage of C···C (*i.e.* π···π) contacts are found in compounds **1f** and **2f**.

Comparison of structures

It is instructive to compare the supramolecular structures of all alcohols in order to understand the supramolecular consequences of molecular changes. The packing arrangement of molecules in a molecular crystal is governed by the interplay of the tendency to close packing and the strength of the intermolecular interactions. As already described above, all new compounds show a large amount of interactions, such as *e.g.*, O–H···N, C–H···O, C/B–H···π and H···H contacts. It is known that from those, the O–H···N are the strongest interactions and they are considered to be moderate hydrogen bonds.[1] This is

Table 3 Geometrical parameters of O–H···N contacts (Å, °), involved in the supramolecular construction of **1,2**

Compounds	O–H···N[a]	*d*(H···N)	*d*(O···N)	∠(OHN)	α^b
1a	(a) O(1)–H···N(1)	2.086	2.900(2)	138.9	—
	(b) O(1)–H···N(1) intramol.	2.455	2.825(3)	101.8	
1c	(c) O(1)–H···N(1)	1.761	2.739(2)	173.0	131
1d	(d) O(1)–H···N(1)	1.748	2.7104(19)	167.1	144
1e	(e) O(1)–H···N(1) intramol.	1.991	2.629(4)	120.4	—
1f	(f) O(1)–H···N(1)	1.763	2.740(2)	172.1	85
2a	(g) O(1A)–H···N(1)	1.780	2.748(2)	167.5	—
2b	(h) O(1)–H···N(1)	1.775	2.713(2)	158.2	—
2c	(i) O(1)–H···N(1)	1.736	2.710(2)	170.2	137
2d	(j) O(1)–H···N(1)	1.692	2.674(4)	175.7	135
2e	(k) O(101)–H···N(101) intramol.	2.068	2.600(4)	111.9	—
	(l) O(201)–H···N(201) intramol.	2.046	2.611(5)	114.4	
2f	(m) O(1)–H···N(1)	1.775	2.689(2)	153.1	121

[a] O–H bond lengths are normalised to neutron distances; See interactions (a) to (m) in Fig. 10–12. [b] The angle between the oxygen atoms of three consecutive molecules in the 1D chains (Fig. 12). Symmetry codes: (c) $x + 1/2, -y + 1/2, z + 1/2$, (d) $1 - x, 0.5 + y, 0.5 - z$, (f) $x + 1/2, -y + 1/2, -z + 1$, (g) $-x, -1/2 + y, 1/2 - z$, (h) $^1/_2 - x, -1/2 + y, ^1/_2 - z$, (i) $x - 1/2, -y + 1/2, z - 1/2$, (j) $x - 1/2, -y + 3/2, z - 1/2$, (m) $x, -y, z - 1/2$.

Table 4 Geometrical parameters of weak D–H···A (A = O, H) contacts (Å,°), involved in the supramolecular construction in **1,2**. For C/B–H···π contacts, geometries are given with respect to the aromatic centroid M

Compound	D–H···A[a]	*d*(H···A)	∠(CHA)	∠(HHB)
1a	C(4)–H···O(1)^{i}	2.424	142.4	—
	C(6)–H···O(1)^{i}	2.682	117.6	—
	C(3)–H(A)···H–B(5)^{ii}	2.075	147.8	133.4
1c	C(7)–H···O(1)^{iii}	2.644	144.0	—
	B(11)–H···M^{iv}		139.8	—
1d	C(9)–H(C)···H–B(8)^{v}	2.127	166.4	116.3
	C(7)–H···H–B(9)^{vi}	2.393	123.0	110.9
1e	O(1)–H···H–B(8)^{vii}	2.184	147.6	128.0
1f	C(3)–H(3B)···H–B(12)^{viii}	2.137	165.7	114.7
	C(3)–H(3A)···H–B(7)^{ix}	2.168	150.7	114.0
	C(4)–H···H(3)–B(3)^{ix}	2.333	159.4	162.2
2a	C(3A)–H···O(1)^{x}	2.274	144.0	—
	C(2)–H···H–B(7)^{xi}	2.355	128.8	146.6
	C(5)–H···H–B(9)^{xii}	2.367	139.9	129.5
2b	C(7)–H···H–B(12)^{xiii}	2.188	157.8	112.2
	C(3)–H···H–B(4)^{xiv}	2.302	118.0	165.9
2c	C(6)–H···O(1)^{xi}	2.577	134.6	—
	B(10)–H···M^{xv}	2.849	138.8	—
	C(3)–H···H–B(8)^{xvi}	2.200	168.5	151.8
	C(5)–H···H–B(10)^{xvii}	2.252	133.7	132.0
	C(7)–H···H–B(12)^{xviii}	2.366	152.5	119.9
2d	C(2)–H···O(1)^{xix}	2.269	168.1	—
	C(8)–H···O(1)^{xix}	2.440	166.3	—
	C(3)–H···H–B(9)^{xx}	2.205	138.0	166.1
	C(3)–H···H–B(12)^{ii}	2.388	127.9	157.1
2e	C(106)–H···O(201)^{xxi}	2.652	140.4	—
	C(206)–H···O(101)^{xxii}	2.616	145.4	—
	C(103)–H···M′^{xxi}	2.737	160.1	—
	C(105)–H···M″^{xxi}	2.652	139.0	—
	C(203)–H···M‴^{xxii}	2.820	157.3	—
	C(205)–H···M⁗^{xxii}	2.663	141.2	—
	O(101)–H···H–B(105)^{xxiii}	2.200	145.1	114.0
	O(201)–H···H–B(205)^{xxiv}	2.127	141.8	114.1
	C(110)–H···H–B(208)	2.241	168.7	109.4
	C(209)–H···H–B(212)^{xxv}	2.390	148.9	106.5
2f	C(6)–H···H–B(9)^{ii}	2.253	117.3	117.2
	C(2)–H···H–B(12)^{xiv}	2.352	141.6	135.7

[a] O–H bond lengths are not normalised to neutron distances. Symmetry codes (i) $0.5 - x, 0.5 - y, 1 - z$; (ii) $x, -1 + y, z$; (iii) $-x, -y, -z$; (iv) $-0.5 + x, 0.5 - y, 0.5 + z$; (v) $0.5 - x, -y, -0.5 + z$; (vi) $x, -0.5 - y, -0.5 + z$; (vii) $2 - x, 1 - y, -z$; (viii) $0.5 + x, y, 0.5 - z$; (ix) $0.5 - x, 0.5 + y, z$; (x) $2 - x, -0.5 + y, 0.5 - z$; (xi) $2 - x, -y, 1 - z$; (xii) $1 - x, -0.5 + y, 0.5 - z$; (xiii) $-0.5 + x, -0.5 + y, z$; (xiv) $0.5 - x, -0.5 + y, 0.5 - z$; (xvi) $2.5 - x, 0.5 + y, 0.5 - z$; (xvii) $2.5 - x, -0.5 + y, 0.5 - z$; (xviii) $x, y, 1 + z$; (xix) $-x, 2 - y, 2 - z$; (xx) $0.5 - x, -0.5 + y, 1.5 - z$; (xxi) $1 - x, 0.5 + y, 1 - z$; (xxii) $-x, -0.5 + y, 1 - z$; (xxiii) $-1 + x, y, z$; (xxiv) $1 + x, y, z$; (xxv) $1 + x, y, 1 + z$.

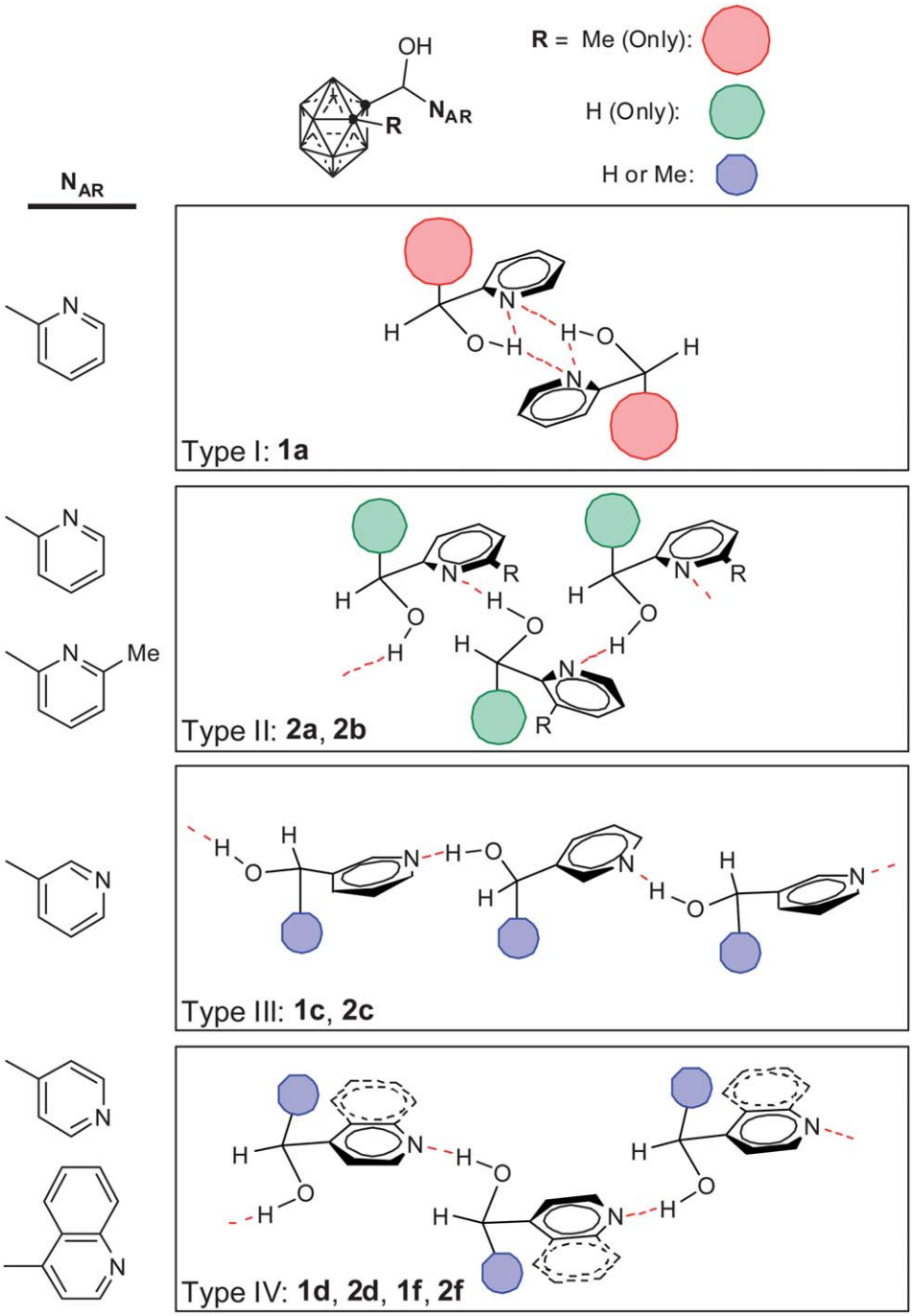

Scheme 4 Summary of molecular structures and corresponding OHN supramolecular heterosynthons.

clear when analysed the present supramolecular structures of all N_{AR} carboranyl alcohols and, together with our previous report, confirms that the O–H···N hydrogen bonds constitute a robust heterosynthon in these molecules. This is summarized in Scheme 4.

Let us first consider the influence of the carboranyl fragments for a given pyridine or quinoline structure (**a**, **b**, **c**, **d** and **f** in Schemes 2 and 4) on the intermolecular O–H···N hydrogen bonds. It can be seen that the O···N distances increase when replacing the *o*-carboranyl by the methyl-*o*-carboranyl fragment, or in other words, by replacing the H atom attached to one of the cage carbons by a bulkier methyl group (Scheme 2). The increase of the intermolecular O···N distances from *o*-carboranyl to methyl-*o*-carboranyl fragment is more significant for the 2-pyridyl (0.15 Å from **2a** to **1a**) than for the 4-quinolyl (0.05 Å from **2f** to **1f**) or than that for the 3- and 4-pyridyl derivatives (0.03 and 0.04 Å, from **2c** to **1c** and from **2d** to **1d**, respectively). The proximity of the methyl group to the OH moiety imposes some limit to the approximation of contiguous molecules and consequently makes, to some extent, the formation of intermolecular

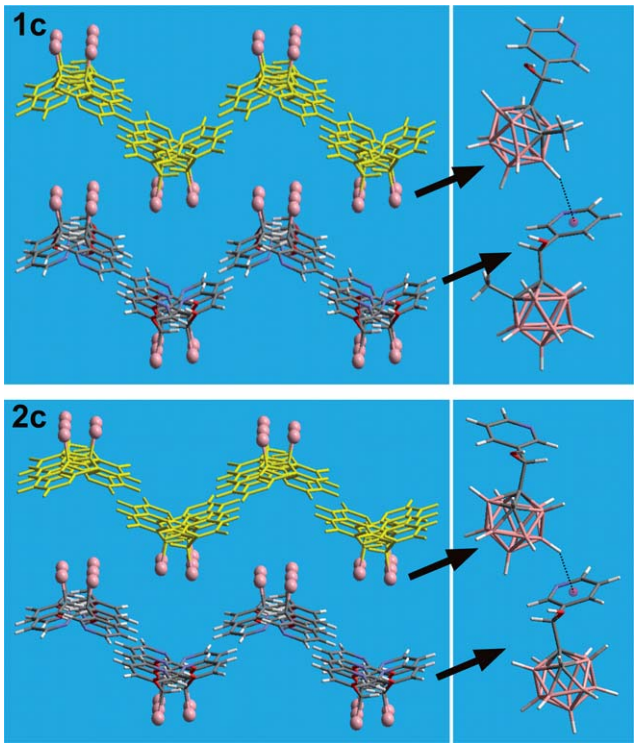

Fig. 13 Projections along the hydrogen bonded networks (along a perspective between *b* and *c* axes) showing the packing of **1c** and **2c**. See text and Table 4 for metric parameters. The carborane cages are replaced by a pink ball in the left diagrams for clarity. Color code: B pink; C grey; H white; O red; N blue.

O–H···N hydrogen bonds difficult (*steric control*). The major difference between the O···N distances in the 2-pyridyl derivatives (0.15 Å) can be explained by the bifurcated nature of the interaction in the case of **1a**, in contrast to the monofurcated nature of that for **2a** (Fig. 10). Let us now consider the influence of the nature of the N_{AR} ring on the O–H···N hydrogen bonds for a given carboranyl fragment. There is a clear decrease of the intermolecular O···N distances from the 2- to the 3- and to the 4-pyridine derivatives, or in other words, the intermolecular O···N distances become shorter as the N atom moves away from the OH moiety in the pyridine series (Table 3). Thus, the intermolecular O···N distances become 0.03–0.04 Å shorter every time that the N atom of the pyridine ring moves one position (from 2- to 3- and from 3- to 4-pyridyl). Again, the 2-pyridyl derivative (**1a**) deviates from this trend due to the bifurcated nature of the hydrogen bond. An interesting apparent deviation to this trend is observed for the intermolecular O···N distance in compound **2b**. This compound can be regarded as the result of substituting the H atom at position-6 of the 2-pyridyl ring in **2a** by a methyl group. The latter certainly increases the bulkiness around the N atom in **2b** and consequently it should affect the formation of intermolecular O–H···N hydrogen bonds, in the direction of increasing the O···N distance. However, the contrary is observed and the intermolecular O···N distance for **2b** is 0.04 Å shorter than that for **2a** and of the same magnitude than that for the 4-pyridine derivative **2c** (Table 3). This deviation can be explained by analysing the O–H···N hydrogen bond angles for all pyridine derivatives. The 6-methyl-2-pyridyl derivative **2b** shows a less linear hydrogen bond (158°) than those for all other pyridine derivatives (~170°). As for the 4-quinolyl compounds (**1f** and **2f**), they can be considered as the result of fusing a phenyl ring to the 4-pyridyl compounds (**1d** and **2d**, respectively; Scheme 2). Intermolecular O···N distances in **1f** and **2f** are 0.02 and 0.03 Å longer than their pyridine counterparts **1d** and **2d**, respectively (Table 3). Analysis of the supramolecular structures suggests that the longer O···N distances for the quinolyl compounds could be due to the presence of π–π stacking

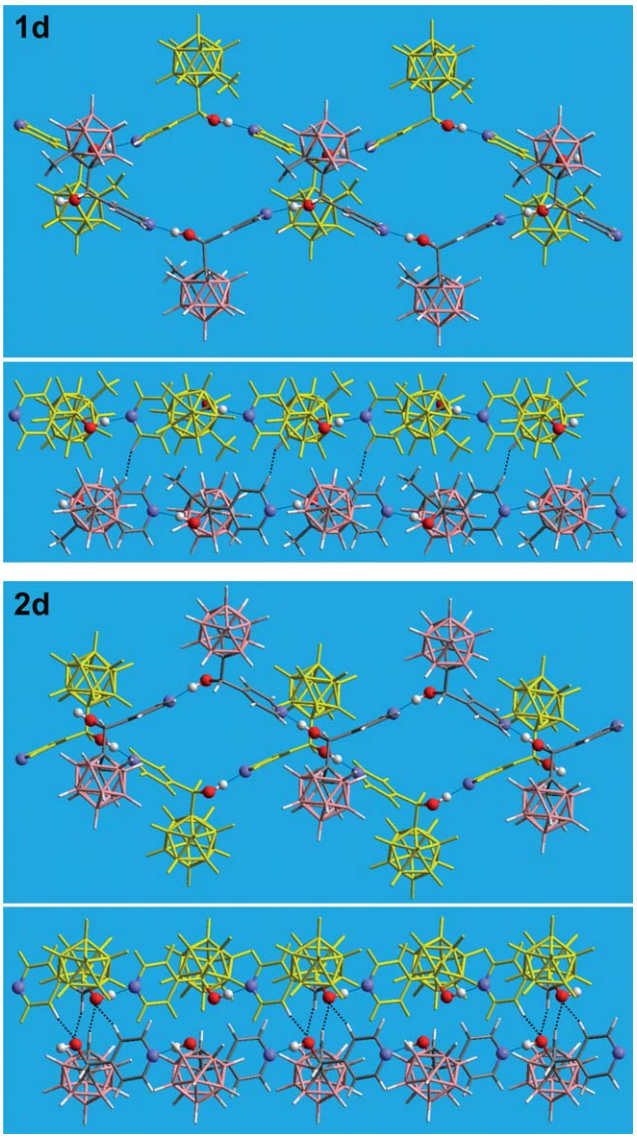

Fig. 14 A comparison of the supramolecular assemblies of **1d** and **2d** showing the intermolecular interactions between O–H···N hydrogen bonded 1D chains. Both structures contain very similar primary supramolecular synthons, namely hydrogen bonded tapes. In **1d** these possess screw symmetry along the axis of the tape, whilst in **2d** they possess glide symmetry. The figure shows how nearest neighbour tapes are arranged in a similar fashion for both structures, however, the extended packing is very different. In **1d** the interlacing of the carborane cages from adjacent tapes involves a 90° rotation producing a step like sequence, whilst in **2d** the interlacing is planar. See Table 4 for metric parameters. Color code: B pink; C grey; H white; O red; N blue.

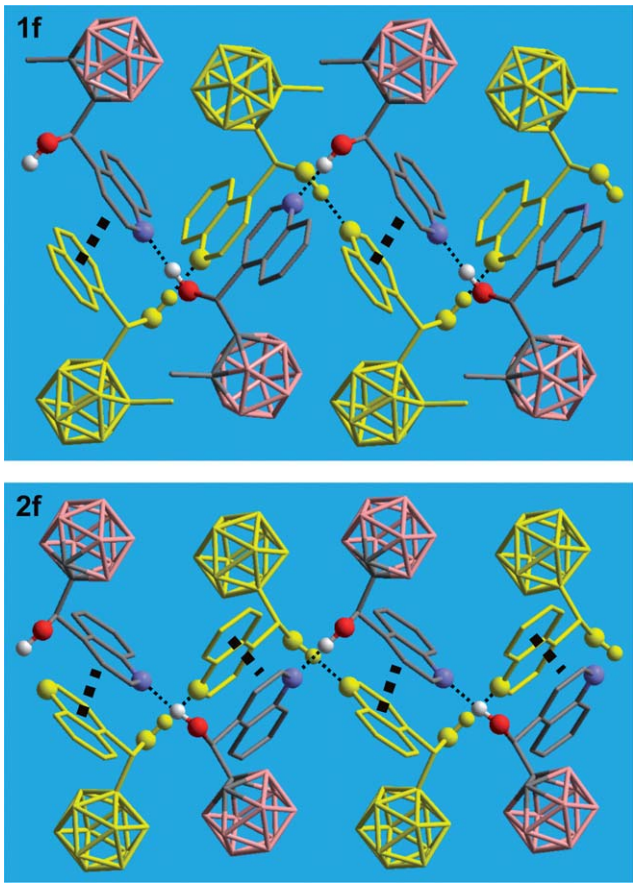

Fig. 15 Supramolecular assemblies of **1f** and **2f**. Representations of the π–π stacking of O–H···N hydrogen bonded networks. All hydrogen atoms, except those for the OH, are omitted for clarity. See text for metric parameters. Color code: B pink; C grey; H white; O red.

interactions rather than to steric effects. The latter clearly affects the O–H···N hydrogen bond angles, so that the methyl-*o*-carboranyl derivative **1f** shows a more linear O–H···N hydrogen bond than for the *o*-carboranyl derivative **2f**.

Vibrational spectroscopy can directly infer the hydrogen bond nature of a given intermolecular interaction. This is done by measuring the X–H stretching frequency ν_{XH} of the desired compound, in the solid state and in an inert solvent. Ideally, ν_{XH} of the undisturbed X–H group should be measured in a solvent as apolar as possible. Unfortunately, all new compounds are insoluble in halogenated solvents and only partially soluble in acetone. Therefore, we have calculated the IR spectra for the optimized structure by DFT (ESI†) of selected compounds (2-pyridyl **1a**, **2a**; 4-pyridyl **1d**, **2d** and 2-quinolyl derivatives **1e**, **2e**). In agreement with the experimental results, the most intense bands correspond to the OH and BH stretching frequencies, which appear at 3681–3503 and 2592–2569 cm^{-1}, respectively. The gas phase calculated stretching frequencies for the OH in the monomers are in the range for non-hydrogen bonded alcohols. Interestingly, calculated IR spectra for dimers of some of the compounds exhibiting intermolecular O–H···N hydrogen bonding **1a**, **2a**, **1d** and **2d** show a clear red shift of the ν_{OH} bands of 66, 131, 400 and 540 cm^{-1}, respectively. Overall, the computed results are in fair agreement with the experimental values (ESI†) and correlate fairly well with the intermolecular O···N distances. Finally, gas phase calculations show that the energy for the O–H···N interactions in hydrogen bonded dimers for the pyridine derivatives is in the range 4–8 kcal mol^{-1}, in good agreement with this type of interactions.[1]

Correlation of melting points with hydrogen bonding networks

The current family of alcohols is chemically inert towards air or water. Chemical and thermal stability are important requirements for practical applications. In general, the melting point of a molecular crystal correlates with its lattice energy. However, this generalization provides no indication of the main factors controlling the melting process. At the melting point the solid and liquid phases exist in equilibrium. Recent studies have shown that it is a subtle and complex interplay of factors such as density, packing features, entropy, molecular structure, and strength and nature of the intermolecular interactions that will determine whether a molecular crystal melts at a relatively low or high temperature.[19] Experimental data show, however, that intermolecular hydrogen bonding increases the melting point. In fact, intuition suggests that hydrogen bonded crystals should have high melting points because the hydrogen bonds hold the molecules together in the crystal.[20] As mentioned above, melting points for all *N*-aromatic carboranyl alcohols in this work were measured by thermal analysis (DTA or DSC and hot-stage microscopy (HSM)) and showed to be in the range 121–256 °C (Table 1 and ESI†). Fig. 18 shows a melting point scale with all *N*-aromatic carboranyl alcohols and that of the related C-aromatic carboranyl alcohols.[4f]

At first glance, it is clear that the lowest melting point compounds correspond to those carboranyl alcohols not having *N*-aromatic rings. As previously reported,[4f] the latter alcohols form supramolecular tetramers sustained by intermolecular O–H···O hydrogen bonds. The inclusion of an aromatic nitrogen in these molecules shifts the supramolecular situation to the more stable O–H···N heterosynthon with the consequent increase in melting points. It is clear that intermolecular interactions in the present group of molecules do appreciably affect their melting points. It is interesting to note that the carboranyl alcohols having the 2-substituted *N*-aromatic rings show considerably lower melting points than the related 3- and 4-substituted compounds. Such melting point differences have been found among highly symmetrical and non-symmetrical isomers.[21] However, we cannot rule out that the melting point difference between these compounds has its origin in the nature of their O–H···N supramolecular networks. In fact, whereas all 2-pyridine derivatives form type I or II supramolecular O–H···N networks, the 3- and 4-pyridine derivatives form type III or IV networks (Scheme 4 and Fig. 18). The low melting points observed for compounds **1e** and **2e** can be explained by the absence of intermolecular O–H···N hydrogen bonds.

As discussed above, the intermolecular O···N distances become shorter as the N atom moves away from the OH moiety in the pyridine series (Table 3). However, although compounds having shorter O···N distances in the crystal show a clear tendency to present higher melting points, these do not correlate well with the O···N distances (R^2 = 0.43, ESI†). This is not unexpected since the strength of a given hydrogen bond has been

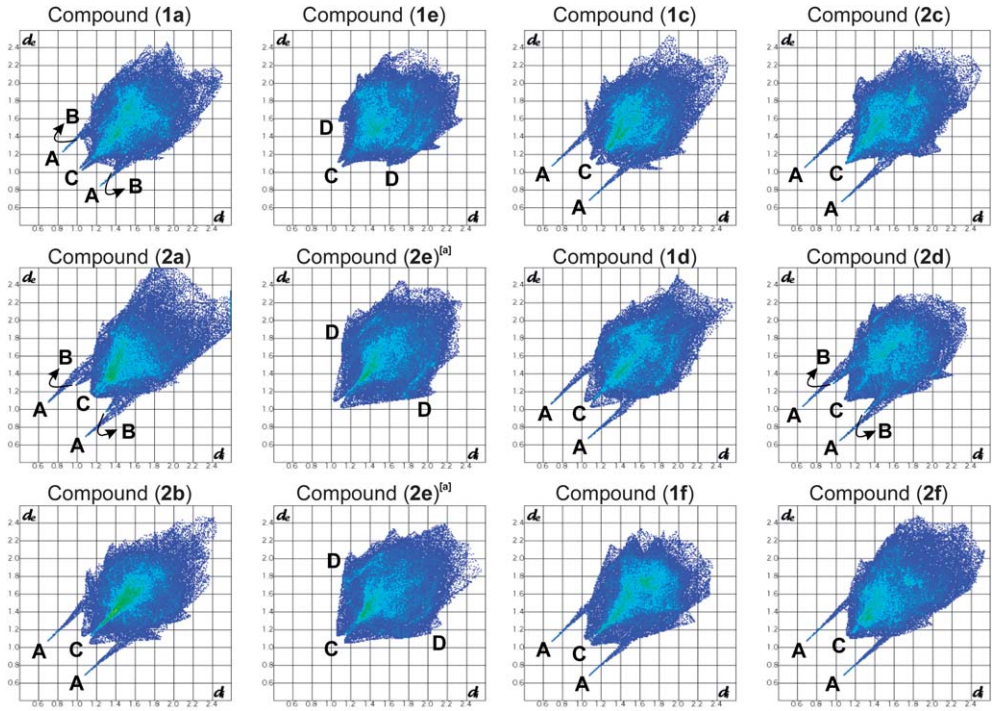

Fig. 16 Comparison between 2D fingerprint plots for all compounds in this study. Nomenclature: A = H···N; B = H···O; C = H···H; D = H···C.[a] Compound **2e** shows two independent molecules in the asymmetric unit.

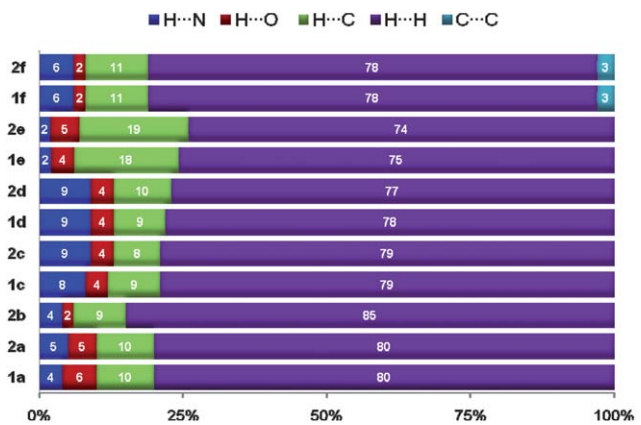

Fig. 17 Relative contributions of various intermolecular contacts to the Hirshfeld surface area in all compounds in this study.

defined on the basis of interaction geometries in the crystal structures, that is, not only short distances but also fairly linear angles (180°).[1] A better correlation is observed for the OHN angles *versus* melting points (R^2 = 0.51, ESI†), but this is still unsatisfactory. Most gratifyingly, we have found a reasonably good correlation between melting points of the pyridine derivatives (**1a**, **1c,d**, **2a–d**) and the relative contribution of the H···N intermolecular contacts to the Hirshfeld surfaces (Fig. 19). No other mp correlation has been found with the relative contribution of all other intermolecular contacts present in these molecules.

It has been found a strong correlation between the symmetry of the molecular van der Waals (vdW) surface and the melting points for molecular crystals of organic compounds that do not have strong electrostatic and specific intermolecular interactions.[22] Indeed, these vdW surfaces are defined by the molecule itself and therefore point to the close contact region around the molecule, which is the influence range of the vdW forces ($\sim r^{-6}$, where r is the intermolecular distance) on the bulk properties of molecular crystals. Although the Hirshfeld surface defines a volume around a molecule in a manner similar to a vdW surface, it is completely different to the latter in the way that the Hirshfeld surface is defined by the molecule *and* the proximity of its nearest neighbours, and hence encodes information about intermolecular interactions in the whole crystal.[18e] Consequently, the relative contribution of different interactions to the Hirshfeld surface encodes information on that particular interaction through the crystal. This probably explains the much better melting point correlation with the relative contribution of the H···N (*i.e.* O–H···N) intermolecular contacts to the Hirshfeld surfaces in our pyridine derivatives than specific single geometric parameters. In fact, Hirshfeld surface analysis indicates that the use of more symmetrical 4- and 3-pyridine or 4-quinolyl derivatives increases the overall total contribution of H···N interactions compared to the less symmetrical derivatives (2-pyridyl or quinolyl), which will contribute to the higher melting point.

Conclusions

A series of novel methyl-*o*-carboranyl and *o*-carboranyl alcohols bearing *N*-aromatic rings (pyridines and quinolines) have been synthesized and their crystal structures have been determined and compared with those related compounds previously synthesized by us. The compounds have been analysed with respect to the influence of the molecular structures on the crystal structure.

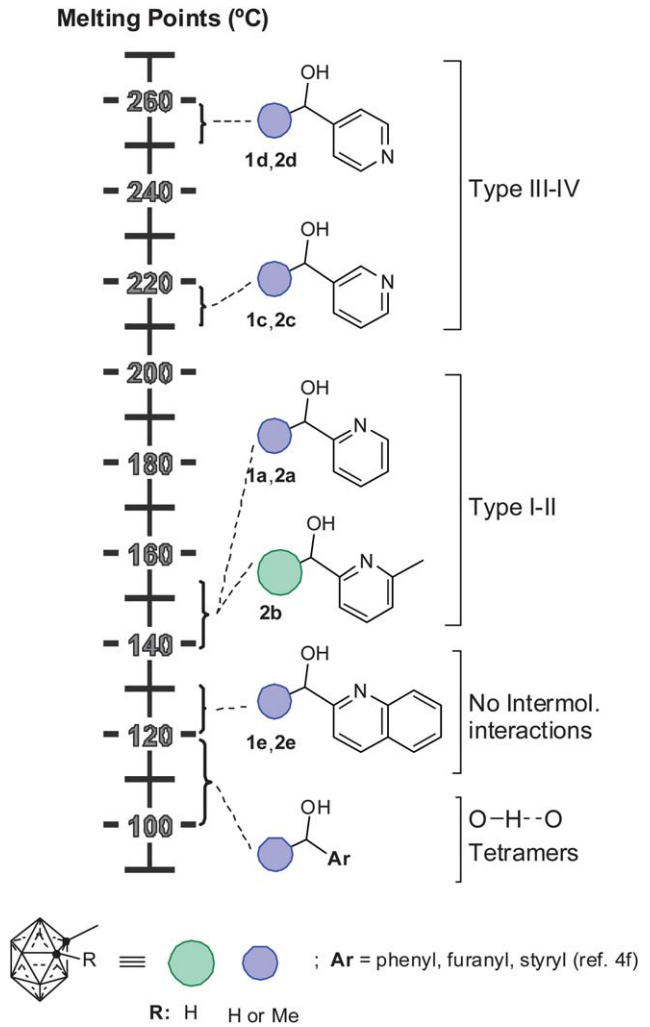

Fig. 18 Melting point scale representation for carboranyl alcohols.

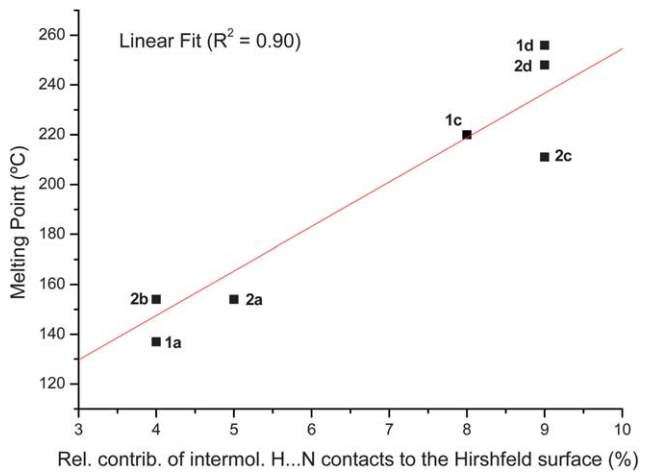

Fig. 19 Plot of observed melting points and corresponding relative contribution of the H···N intermolecular contacts to the Hirshfeld surfaces.

Analysis of their supramolecular structures, both manually and with the aid of Hirshfeld surface analysis and decomposed fingerprint plots, shows that the compounds share some similar supramolecular features: O–H···N, C–H···O hydrogen bonds, H···H contacts and some degree of (C/B)–H···π interactions. Overall, O–H···N hydrogen bond is the dominant interaction and constitutes a robust heterosynthon in these molecules. Hirshfeld surface analysis indicates that the use of more symmetrical 4- and 3-pyridine or 4-quinolyl derivatives increases the overall total contribution of H···N interactions compared to the less symmetrical derivatives (2-pyridyl or quinolyl), which will contribute to the higher melting point. Finally, we have been able to correlate the presence of an infinite O–H···N hydrogen bonding network in the crystal structure for the pyridine compounds with their melting points. Based on the present results, we suggest that the analysis of Hirshfeld surface and decomposed fingerprint plots opens a new way of interpretation of the observed trends in melting point and probably other properties that are strongly related to intermolecular interactions. The present work establishes reliable connections between structures of *N*-aromatic *o*-carboranyl alcohols and their melting points and has important implications in the structure–property relationships in these compounds in particular, and structural chemistry in general. These observations also serve in the understanding of the basic principles of supramolecular chemistry of *o*-carboranyl systems and, consequently, for the progress of crystal engineering.

Experimental section

General remarks

Reactions were carried out under a nitrogen atmosphere in round-bottomed flasks equipped with a magnetic stirring bar, capped with a septum. THF and diethyl ether were distilled from Na/benzophenone and CH_2Cl_2 over CaH_2. All the other chemicals were commercially available and used as received. Compounds **1a** and **1d** were synthesized according to the literature.[4f,11a] TLC analyses were performed on Merck silica gel 60 F_{254} TLC plates (0.5 mm thickness). Melting points were measured on a Stuart Scientific SMP10 and/or a Büchi Melting-Point B545. IR spectra were recorded from KBr pellets on a Perkin-Elmer Spectrum One spectrometer. ^{1}H, ^{13}C and ^{11}B spectra were recorded respectively at 300, 75 and 96 MHz with a Bruker Advance-300 spectrometer in deuterated acetone, unless denoted, and referenced to the residual solvent peak for ^{1}H and ^{13}C NMR or to $BF_3{\cdot}OEt_2$ as an external standard for ^{11}B NMR. Chemical shifts are reported in ppm and coupling constants in Hertz. Multiplets nomenclature is as follows: s, singlet; d, doublet; t, triplet; br, broad; m, multiplet. Elemental analyses were obtained by a CarboErba EA1108 microanalyzer (Universidad Autónoma de Barcelona). Samples for thermogravimetric characterization were placed in open alumina crucibles and analyzed using a NETZSCH STA 449F1 thermobalance operating under nitrogen. A heating rate of 10 °C min^{-1} was used and all samples (8–13 mg) were studied between 40 and 1000 °C. Hot stage microscopy (HSM) examinations were performed on a Linkam THMS-600 heating–freezing stage equipped with a video. Calibration was performed with the appropriate chemicals from Merck Corporation. Due to partial sublimation of the compounds before melting, the heating plate was not closed during the heating runs with a consequential loss of accuracy (about ±5–10 °C).

(6-Methyl-2-pyridine)(methyl-*o*-carboranyl)methanol (1b)

An analogue procedure to that previously reported was followed,[4f,11a] using methyl-*o*-carborane (203 mg, 1.28 mmol), *n*-BuLi (0.8 mL, 1.6 M in hexane, 1.28 mmol) and 6-methyl-2-pyridinecarboxaldehyde (155 mg, 1.28 mmol).

Evaporation of the solvent gave **1b** as a white solid that was dried under vacuum (163 mg, 0.58 mmol, 45%); mp 106–108 °C, $R_f = 0.87$, hexane : ethyl acetate (1.5 : 2). ^{1}H NMR: $\delta = 7.76$ (t, $J = 7.7$, 1H, $CH_3C_5H_3N$), 7.39 (d, $J = 7.7$, 1H, $CH_3C_5H_3N$), 7.27 (d, $J = 7.6$, 1H, $CH_3C_5H_3N$), 5.78 (d, $J = 7.3$, 1H, CHO*H*), 5.30 (d, $J = 6.8$, 1H, C*H*OH), 2.54 (s, 3H, $CcCH_3$), 2.34 (s, 3H, $CH_3C_5H_3N$). ^{1}H{^{11}B} NMR (only the new signals due to B–H protons are listed): $\delta = 2.78$ (br s, 1H), 2.65 (br s, 1H), 2.45–2.16 (br m, 5H), 1.95 (br s, 1H), 1.91 (br s, 1H), 1.44 (br s, 1H). ^{13}C NMR: $\delta = 22.88$, 23.31, 62.73, 72.74, 75.95, 83.44, 119.60, 123.22, 137.03, 157.23. ^{11}B NMR: $\delta = -2.6$ (d, $J_{B,H} = 148$, 1B), -5.4 (d, $J_{B,H} = 149$, 1B), -7 and -13 (m, 8B). IR (in KBr; only assigned bands are listed here and in Table 1; see ESI† for complete spectrum): $\nu = 2594$ (BH). $C_{10}H_{21}B_{10}ON$ (315.44): calcd C 42.99, H 7.58, N 5.01; found C 43.03, H 7.78, N 4.85%.

(3-Pyridine)(methyl-*o*-carboranyl)methanol (1c)

An analogue procedure to that previously reported was followed,[4f,11a] using methyl-*o*-carborane (303 mg, 1.916 mmol), *n*-BuLi (1.22 mL, 1.57 M in hexane, 1.916 mmol) and 3-pyridinecarboxaldehyde (209.5 mg, 0.183 mL, 1.916 mmol). The crude product precipitated from the reaction mixture in the fridge was washed with hexane and dried under vacuum to obtain pure **1c** as a white solid (319.6 mg, 1.20 mmol, 62%); mp 210 °C (dec.), $R_f = 0.08$, hexane : ethyl acetate (1 : 1). ^{1}H NMR: $\delta = 8.68$ (d, $J = 2.0$, 1H, C_5H_4N), 8.57 (dd, $J = 4.8$, 1.6 Hz, 1H, C_5H_4N), 8.01–7.84 (m, 1H, C_5H_4N), 7.42 (dd, $J = 7.9$, 4.8, 1H, C_5H_4N), 6.02 (d, $J = 5.1$, 1H, CHO*H*), 5.49 (d, $J = 4.8$, 1H, C*H*OH), 2.34 (s, 3H, $CcCH_3$). ^{1}H{^{11}B} NMR (only the new signals due to B–H protons are listed): $\delta = 2.76$ (br s, 1B), 2.49–2.09 (m, 6B), 1.98 (br s, 1B), 1.89 (br s, 1B), 1.37 (br s, 1B). ^{13}C NMR: $\delta = 22.65$, 44.52, 70.77, 82.28, 123.14, 134.73, 136.58, 148.75, 149.89. ^{11}B NMR: $\delta = -2.4$ (d, $J_{B,H} = 148$, 1B), -5.2 (d, $J_{B,H} = 151$, 1B), -7 and -14 (m, 8B). IR (in KBr; only assigned bands are listed here and in Table 1; see ESI† for complete spectrum): $\nu = 2570$ (BH). $C_9H_{19}B_{10}ON$ (265.38): calcd C 40.74, H 7.22, N 5.28; found C 39.98, H 7.19, N 5.96%.

(2-Quinoline)(methyl-*o*-carboranyl)methanol (1e)

An analogue procedure to that previously reported was followed,[4f,11a] using methyl-*o*-carborane (313.7 mg, 1.98 mmol), *n*-BuLi (1.27 mL, 1.56 M in hexane, 1.98 mmol) and 2-quinolinecarboxaldehyde (320.8 mg, 1.98 mmol). Addition of the aldehyde to the lithium salt of the methyl-*o*-carborane was followed by a persistent intense blue color that only disappeared after the addition of the saturated ammonium chloride water solution. The crude product after evaporation was washed with pentane giving pure **1e** as a pale orange solid (359.6 mg, 1.14 mmol, 57%); mp 108–112 °C (dec.), $R_f = 0.73$, chloroform : ethyl acetate (3 : 1). ^{1}H NMR: $\delta = 8.44$ (d, $J = 8.5$, 1H, C_9H_6N), 8.07 (d, $J = 8.4$, 1H, C_9H_6N), 8.01 (d, $J = 8.1$, 1H, C_9H_6N), 7.86–7.71 (m, 2H, C_9H_6N), 7.65 (t, $J = 7.0$, 1H, C_9H_6N), 6.17 (d, $J = 6.4$, 1H, CHO*H*), 5.55 (d, $J = 5.5$, 1H, C*H*OH), 2.40 (s, 3H, $CcCH_3$). ^{1}H{^{11}B} NMR (only the new signals due to B–H protons are listed): $\delta = 2.73$ (br s, 1B), 2.45 (br s, 1B), 2.31–1.98 (m, 5B), 1.92 (br s, 1B), 1.87 (br s, 1B), 1.39 (br s, 1B). ^{13}C RMN: $\delta = 22.90$, 73.38, 76.13, 83.00, 120.09, 127.16, 127.88, 128.12, 128,98, 129.98, 136.89, 146.54, 158.59. ^{11}B NMR: $\delta = -2.4$ (d, $J_{B,H} = 148$ Hz, 1B), -5.4 (d, $J_{B,H} = 149$ Hz, 1B), -7 and -14 (m, 8B). IR (in KBr; only assigned bands are listed here and in Table 1; see ESI† for complete spectrum): $\nu = 2594$–2553 (BH). $C_{13}H_{21}B_{10}ON$ (315.44): calcd C 40.50, H 6.71, N 4.44; found 50.37, H 6.67, N 4.39%.

(4-Quinoline)(methyl-*o*-carboranyl)methanol (1f)

An analogue procedure to that previously reported was followed,[4f,11a] using methyl-*o*-carborane (316.7 mg, 2.00 mmol), *n*-BuLi (1.28 mL, 1.56 M in hexane, 2.00 mmol) and 4-quinolinecarboxaldehyde (324 mg, 2.00 mmol). The crude product precipitated from the reaction mixture in the fridge was washed with hexane and dried under vacuum to obtain pure **1f** as a white solid (496 mg, 1.57 mmol, 78%); $R_f = 0.4$, chloroform : ethyl acetate (1 : 1). ^{1}H NMR: $\delta = 8.99$ (d, $J = 4.5$, 1H, C_9H_6N), 8.40 (br s, 1H, C_9H_6N), 8.12 (d, $J = 8.6$, 1H, C_9H_6N), 7.91–7.75 (m, 2H, C_9H_6N), 7.73–7.60 (m, 1H, C_9H_6N), 6.30 (br s, 1H, CHO*H*), 6.17 (br s, 1H, C*H*OH), 2.48 (s, 3H, $CcCH_3$). ^{1}H{^{11}B} NMR (only the new signals due to B–H protons are listed): $\delta = 2.97$ (br s, 1B), 2.65 (br s, 1B), 2.44–1.99 (m, 5B), 1.91 (br s, 1B), 1.80 (br s, 1B), 1.11 (br s, 1B). ^{13}C NMR: $\delta = 22.85$, 75.95, 82.41, 120.96, 124.01, 125.88, 126.71, 129.14, 130.33, 145.98, 148.55, 149.93, 150.38. ^{11}B NMR: $\delta = -2.4$ (d, $J_{B,H} = 147$, 1B), -5.1 (d, $J_{B,H} = 150$, 1B), -7 and -14 (m, 8B). IR (in KBr; only assigned bands are listed here and in Table 1; see ESI† for complete spectrum): $\nu = 2630$–2575 (BH). $C_{13}H_{21}B_{10}ON$ (315.44): calcd C 40.50, H 6.71, N 4.44; found 50.73, H 6.85, N 4.33%.

General procedure for the synthesis of *o*-carboranylmethanols 2a–f

*n*BuLi (1.6 M in hexane, 1.00 mmol) was added dropwise to a diethyl ether solution (20 mL) of the appropriate *o*-carborane (1.00 mmol) at −84 °C (ethyl acetate/liq. N_2 bath). The mixture was stirred for 1 hour at low temperature giving a clear pale yellow solution. Then a diethyl ether solution (5 mL) of the aldehyde (1.00 mmol) was added. The resulting yellow solution was stirred at −84 °C and the reaction was monitored by TLC. After the reaction was complete (typically around 4–5 hours), a saturated aqueous solution of NH_4Cl (10 mL) was added at −84 °C and then the mixture was taken out of the cooling bath and let to stir till it reaches room temperature. The aqueous phase was then extracted with Et_2O (3 × 20 mL) and the combined organic phases were dried over $MgSO_4$ and filtered. Slow evaporation of the concentrated solution afforded the pure desired alcohols as crystalline materials suitable for X-ray determination in most of the cases.

(2-Pyridine)(*o*-carboranyl)methanol (2a)

The general procedure was followed, using *o*-carborane (319.3 mg, 2.21 mmol), *n*-BuLi (1.43 mL, 1.55 M, 2.21 mmol) and 2-pyridinecarboxaldehyde (239.4 mg, 0.21 mL, 2.21 mmol). The

residue was washed with hexane–ethanol mixture to eliminate the colored impurities to obtain pure **2a** as crystalline pale yellow solid (419 mg, 1.66 mmol, 75%); mp 153–156 °C (dec.), $R_f = 0.18$, hexane : ethyl acetate (1.5 : 1). ^{1}H NMR: $\delta = 8.58$ (dd, $J = 3.1$, 0.9 Hz, 1H, C_5H_4N), 7.89 (td, $J = 7.7$, 1.7 Hz, 1H, C_5H_4N), 7.57 (d, $J = 7.9$ Hz, 1H, C_5H_4N), 7.41 (ddd, $J = 7.6$, 4.9, 1.2 Hz, 1H, C_5H_4N), 5.96 (d, $J = 7.0$ Hz, 1H, CHO*H*), 5.36 (d, $J = 7.0$ Hz, 1H, C*H*OH), 4.74 (s, 1H, C*c*H). ^{1}H{^{11}B} RMN (only the new signals due to B–H protons are listed): $\delta = 2.45$ (br s, 1B), 2.35 (br s, 1B), 2.23 (br s, 1B), 2.19–2.03 (br m, 5B), 2.00 (br s, 1B), 1.63 (br s, 1B). ^{13}C NMR: $\delta = 59.80$, 74.00, 79.82, 122.09, 124.06, 137.01, 148.47, 157.67. ^{11}B NMR: $\delta = -2.8$ (d, $J_{B,H} = 134$, 1B), −4.2 (d, $J_{B,H} = 125$, 1B), −7 and −15 (m, 8B). IR (in KBr; only assigned bands are listed here and in Table 1; see ESI† for complete spectrum): ν = 3084 (C*c*H), 2594 (BH). $C_8H_{17}B_{10}ON$ (251.34): calcd C 38.23, H 6.82, N 5.57; found C 37.81, H 6.78, N 5.35%.

(6-Methyl-2-pyridine)(*o*-carboranyl)methanol (2b)

The general procedure was followed, using *o*-carborane (311.3 mg, 2.15 mmol), *n*-BuLi (1.35 mL, 1.6 M, 2.15 mmol) and 6-methyl-2-pyridinecarboxaldehyde (261.5 mg, 2.15 mmol). The residue was washed with hexane to obtain pure **2b** as a white crystalline solid (447 mg, 1.68 mmol, 78%); mp 160 °C (dec.), $R_f = 0.6$, hexane : ethyl acetate (1 : 1). ^{1}H NMR: $\delta = 7.76$ (t, $J = 7.7$, 1H, $CH_3C_5H_3N$), 7.34 (d, $J = 7.6$, 1H, $CH_3C_5H_3N$), 7.28 (d, $J = 7.7$, 1H, $CH_3C_5H_3N$), 5.90 (d, $J = 7.1$, 1H, CHO*H*), 5.30 (d, $J = 6.8$, 1H, C*H*OH), 4.41 (s, 1H, C*c*H), 2.52 (s, 3H, $CH_3C_5H_3N$). ^{1}H {^{11}B} NMR (only the new signals due to B–H protons are listed): $\delta = 2.46$ (br s, 1B), 2.33 (br s, 1B), 2.24 (br s, 1B), 2.21–2.00 (br m, 6B), 1.66 (br s, 1B). ^{13}C NMR: $\delta = 23.31$, 59.74, 73.65, 79.98, 119.18, 123.41, 137.22, 156.45, 157.46. ^{11}B NMR: $\delta = -2.8$ (d, $J_{B,H} = 135$, 1B), −4.2 (d, $J_{B,H} = 128$, 1B), −7 and −15 (m, 8B). IR (in KBr; only assigned bands are listed here and in Table 1; see ESI† for complete spectrum): $\nu = 3086$ (C*c*H), 2621–2578 (BH). $C_9H_{19}B_{10}ON$ (301.39): calcd C 40.74, H 7.22, N 5.80; found C 41.62, H 7.26, N 5.31%.

(3-Pyridine)(*o*-carboranyl)methanol (2c)

The general procedure was followed, using *o*-carborane (189.9 mg, 1.316 mmol), *n*-BuLi (0.82 mL, 1.6 M, 1.316 mmol) and 3-pyridinecarboxaldehyde (143.91 mg, 0.126 mL, 1.316 mmol). The residue was washed with hexane and dichloromethane to eliminate the colored impurities to obtained pure **2c** as crystalline pale yellow solid (265 mg, 1.05 mmol, 80%); mp 208–210 °C (dec.), $R_f = 0.22$, hexane : ethyl acetate (1 : 1). ^{1}H NMR: $\delta = 8.61$ (d, $J = 2.2$, 1H, C_5H_4N), 8.57 (dd, $J = 4.8$, 1.6, 1H, C_5H_4N), 7.84 (dt, $J = 7.9$, 2.0, 1H, C_5H_4N), 7.41 (ddd, $J = 7.9$, 4.8, 0.6, 1H, C_5H_4N), 6.29 (d, $J = 4.8$, 1H, CHO*H*), 5.51 (d, $J = 3.9$, 1H, C*H*OH), 4.78 (s, 1H, C*c*H). ^{1}H{^{11}B} NMR (only the new signals due to B–H protons are listed): $\delta = 2.79$ (br s, 1B), 2.51 (br s, 1B), 2.40 (br s, 1B), 2.24–1.65 (m, 6B,), 1.59 (br s, 1B). ^{13}C NMR: $\delta = 60.17$, 72.09, 80.11, 123.14, 134.34, 135.83, 148.42, 150.02. ^{11}B NMR: $\delta = -3.6$ (d, $J_{B,H} = 134$, 1B), −4.9 (d, $J_{B,H} = 106$, 1B), −7 and −16 (m, 8B). IR (in KBr; only assigned bands are listed here and in Table 1; see ESI† for complete spectrum): ν = 3082 (C*c*H), 2586 (BH). $C_8H_{17}B_{10}ON$ (251.34): calcd C 38.23, H 6.82, N 5.57; found C 39.00, H 6.99, N 5.63%.

(4-Pyridine)(*o*-carboranyl)methanol (2d)

The general procedure was followed, using *o*-carborane (168 mg, 1.16 mmol), *n*-BuLi (0.8 mL, 1.5 M in hexane, 1.17 mmol), diethyl ether (20 ml) and 4-pyridinecarboxaldehyde (0.11 ml, 1.17 mmol). The residue was washed with CH_2Cl_2 (3 × 5 ml) to obtaine pure **2d** as a white solid (190 mg, 0.75 mmol, 75%); mp: 211 °C (dec.). ^{1}H NMR: $\delta = 8.60$ (dd, ^2J(H,H) = 1.5, ^1J(H,H) = 5.7, 2H, C_5H_4N), 7.42 (ddd, ^1J(H,H) = 4.4, ^2J(H,H) = 1.7, ^3J(H, H) = 0.6, 2H, C_5H_4N), 6.37 (br s, 1H, CHO*H*), 5.45 (br s, 1H, C*H*OH), 4.77 (br s, 1H, C*c*-H). ^{1}H{^{11}B} NMR: only signals due to B–H protons are given: $\delta = 2.50$ (br s, 1H), 2.38 (br s, 1H), 2.17 (br s, 3H), 2.09 (br s, 3H), 1.61 (br s, 1H). ^{11}B NMR: $\delta = -3.8$ (m, 2B), −12.2 (br m, 8B). ^{13}C{^{1}H} NMR [$(CD_3)_2(CO)$]: 150.7, 149.0, 122.8 (NC_5H_4), 80.2 (C*c*), 73.7 (CHOH), 61.1 (C*c*). IR (in KBr; only assigned bands are listed here and in Table 1; see ESI† for complete spectrum): $\nu = 3081$ (C*c*H), 2586–2638 (BH). Anal. calcd for $C_8B_{10}H_{17}NO$ (251.34): C 38.23, H 6.82, N 5.57; found C 38.35, H 7.01; N 5.67%.

(2-Quinoline)(*o*-carboranyl)methanol (2e)

The general procedure was followed, using *o*-carborane (219.8 mg, 1.524 mmol), *n*-BuLi (1.00 mL, 1.52 M, 1.524 mmol) and 2-quinolinecarboxaldehyde (240.33 mg, 1.524 mmol). Addition of the aldehyde to the lithium salt of the *o*-carborane was followed by a persistent intense blue colour that only disappeared after the addition of the saturated ammonium chloride water solution. Compound **2e** was obtained as a light orange solid (383 mg, 1.27 mmol, 83%) by column chromatography (eluent: hexane/ethyl acetate 1 : 1; $R_f = 0.62$); mp 116–118 °C (dec.). ^{1}H NMR: $\delta = 8.45$ (d, $J = 8.6$, 1H, C_9H_6N), 8.06 (d, $J = 8.4$ Hz, 1H, C_9H_6N), 8.02 (d, $J = 8.1$ Hz, 1H, C_9H_6N), 7.82 (ddd, $J = 8.4$, 6.9. 1.5, 1H, C_9H_6N), 7.72 (d, $J = 8.5$, 1H, C_9H_6N), 7.66 (ddd, $J = 8.1$, 6.9, 1.2, 1H, C_9H_6N), 6.25 (d, $J = 6.8$, 1H, CHO*H*), 5.55 (d, $J = 6.7$, 1H, C*H*OH), 4.83 (s, 1H, C*c*H). ^{1}H {^{11}B} NMR (only the new signals due to B–H protons are listed): $\delta = 2.54$ (br s, 1B), 2.43 (br s, 1B), 2.34 (br s, 1B), 2.28–1.98 (m, 6B), 1.66 (br s, 1B).^{13}C RMN: $\delta = 59.82$, 74.20, 79.45, 119.53, 127.10, 127.81, 128.08, 128.89, 129.96, 137.04, 146.45, 157.73. ^{11}B NMR: $\delta = -2.8$ (d, $J_{B,H} = 136$ Hz, 1B), −4.1 (d, $J_{B,H} = 115$ Hz, 1B), −7 and −15 (m, 8B). IR (in KBr; only assigned bands are listed here and in Table 1; see ESI† for complete spectrum): $\nu =$ 3074 (C*c*H), 2582 (BH). $C_{12}H_{19}B_{10}ON$ (301.39): calcd C 47.82, H 6.35, N 4.65; found C 47.61, H 6.26, N 4.49%.

(4-Quinoline)(*o*-carboranyl)methanol (2f)

The general procedure was followed, using *o*-carborane (162.7 mg, 1.128 mmol), *n*-BuLi (0.727 mL, 1.55 M, 1.128 mmol) and 4-quinolinecarboxaldehyde (182.77 mg, 1.128 mmol). The residue was washed with diethyl ether to eliminate the colored impurities to obtain **2f** as light orange crystals (212.6 mg, 0.705 mmol, 62%); $R_f = 0.38$, chloroform : acetone (2 : 1). ^{1}H NMR: $\delta = 8.89$ (d, $J = 4.5$, 1H, C_9H_6N), 8.27 (br d, $J = 7.8$, 1H, C_9H_6N), 8.11 (d, $J = 8.4$, 1H, C_9H_6N), 7.85–7.55 (m, 3H, C_9H_6N), 6.53 (br s, 1H, CHO*H*), 6.32 (br s, 1H, C*H*OH), 4.97 (s,

1H, C*cH*). $^{1}H\{^{11}B\}$ NMR (only the new signals due to B–H protons are listed): $\delta = 2.68$ (br s, 1B), 2.47 (br s, 1B), 2.28 (br s, 1B), 2.22–1.85 (m, 6B), 1.47 (br s, 1B). ^{13}C NMR: $\delta = 60.67$, 68.67, 79.52, 119.82, 123.75, 125.72, 126.74, 129.21, 130.22, 145.45, 148.42, 149.98. ^{11}B NMR: $\delta = -2$ and -6 (m, 2B), -7 and -16 (m, 8B). IR (in KBr; only assigned bands are listed here and in Table 1; see ESI† for complete spectrum): $\nu = 3086$ (C*cH*), 2629 (BH). $C_{12}H_{19}B_{10}ON$ (301.39): calcd C 47.82, H 6.35, N 4.65; found C 48.63, H 6.56, N 4.46%.

Computational details

Gas phase DFT calculations were carried out using the GAUSSIAN 03 software package.[23] Geometries were fully optimized at the B3LYP[24] level with 6-311 + G** basis sets for the isolated molecules (monomers).[25] In order to reduce the computational cost, we employed DZVP basis sets[26] for the optimizations and IR calculations of dimers. Single point energy calculations of the crystal structures were performed at B3LYP/6-311 + G** level of theory and normal modes analysis was performed in order to obtain vibrational frequencies, force constants and zero-point energy corrections for the total energy. Hydrogen bond intermolecular interactions were estimated from the subtraction between the energy of the dimer and two monomer molecules.

X-Ray crystallography

For all compounds, cell dimensions and intensity data were recorded at 120 K, using a Bruker Nonius APEXII (**1c**, **2c**, **2d**, **2e**) or a KappaCCD Roper (**1e**, **1f**, **2b**, **2f**,**2a**) area detector diffractometer mounted at the window of a rotating Mo anode (λ(Mo-Kα) = 0.71073 Å) operating at 50 kV, 85 mA. The incident beam on the APEXII side was focused using 10 cm confocal mirrors, a graphite monochromator was employed on the KappaCCD side. Unit cell determination, data collection and processing were carried out using the programs DirAx,[27] COLLECT[28] and DENZO[29] and a multi-scan absorption correction was applied using SADABS.[30]

The structures were solved *via* direct methods[31] and refined by full matrix least squares[31] on F^2. The treatment of the OH hydrogen atoms is addressed in the *Molecular structures* section of the paper, all C–H and B–H hydrogens were placed in idealised positions and refined using a riding model. CH_3 groups were constrained to be rigid with a refined torsion angle, with the exception of **1f** where convergence was only achieved using a staggered geometry for the methyl group. **1e** was a non-merohedral twin and an *hklf*5 reflection file was prepared using EVAL-14.[32] **2e** has a β angle close to 90° and was refined as a pseudo-merohedral twin, monoclinic emulating orthorhombic, twin law [100 0$\bar{1}$0 00$\bar{1}$], the twin fraction refined to *ca.* 17%. **2a** showed disorder where the position of the OH on the linking carbon is disordered over the 2 possible positions (85 : 15), the atomic displacement parameters for the split oxygen site were restrained to be identical, no geometrical restraints were necessary.

Acknowledgements

We thank CICYT (Project CTQ2010-16237) and Generalitat de Catalunya (2009/SGR/00279) and CSIC (PIE ref. 200860I097) for financial support, and the Centro Técnico de Informática (CSIC) and Centre de Supercomputació de Catalunya (CESCA) for computing support. We also thank Prof. E. Cardellach (Departament de Geologia, Universitat Autònoma de Barcelona) for letting us use the Hot Stage Microscope. FDS thanks CSIC for JAEDOC grant (JAEDoc_08_00332) and CONICET for support.

References

1 See for example: (*a*) G. R. Desiraju, *Crystal Engineering. The Design of Organic Solids*, Elsevier Science Publishers B.V., Amsterdam, 1989; (*b*) M. C. Etter, *Acc. Chem. Res.*, 1990, **23**, 120; (*c*) G. R. Desiraju and T. Steiner, *The Weak Hydrogen Bond in Structural Chemistry and Biology*, Oxford University Press, Oxford, 2001; (*d*) T. Steiner, *Angew. Chem.*, 2002, **114**, 50; *Angew. Chem., Int. Ed.* 2002, 41, 48; (*e*) J. L. Atwood and J. W. Steed, *Encyclopedia of Supramolecular Chemistry*, Marcel Dekker, New York, 2004; (*f*) P. Metrangolo, H. Neukirch, T. Pilati and G. Resnatti, *Acc. Chem. Res.*, 2005, **38**, 386; (*g*) S. Kitagawa and K. Uemura, *Chem. Soc. Rev.*, 2005, **34**, 109; (*h*) D. A. Britz and A. N. Khlobystov, *Chem. Soc. Rev.*, 2006, **35**, 637; (*i*) J. W. Steed and J. L. Atwood, *Supramolecular Chemistry*, Wiley, Chichester, 2nd edn, 2009.

2 F. Teixidor, *J. Organomet. Chem.*, 2009, **694**, 1587.

3 An ISI Web of Knowledge search for the topic "crystal engineering" for all available years (1899–present) afforded 4585 hits. A further search within the latter hits for the words "boron", "carboranes" or metallacarboranes yielded 22, 7 or 1 hits, respectively.

4 (*a*) G. Barberá, C. Viñas, F. Teixidor, G. M. Rosair and A. J. Welch, *J. Chem. Soc., Dalton Trans.*, 2002, 3647; (*b*) J. G. Planas, C. Viñas, F. Teixidor, A. Comas-Vives, G. Ujaque, A. Lledós, M. E. Light and M. B. Hursthouse, *J. Am. Chem. Soc.*, 2005, **127**, 15976; (*c*) J. G. Planas, C. Viñas, F. Teixidor, M. E. Light and M. B. Hursthouse, *CrystEngComm*, 2007, **9**, 888; (*d*) J. G. Planas, F. Teixidor, C. Viñas, M. E. Light and M. B. Hursthouse, *Chem.–Eur. J.*, 2007, **13**, 2493; (*e*) A. V. Puga, F. Teixidor, R. Sillanpää, R. Kivekäs and C. Viñas, *Chem.–Eur. J.*, 2009, **15**, 9755; (*f*) V. Terrasson, Y. García, P. Farràs, F. Teixidor, C. Viñas, J. G. Planas, D. Prim, M. E. Light and M. B. Hursthouse, *CrystEngComm*, 2010, **12**, 4109.

5 See for example (*a*) R. N. Grimes, *Carbaboranes*, Academic Press, New York, 1970, p. 54; (*b*) V. I. Bregadze, *Chem. Rev.*, 1992, **92**, 209; (*c*) J. Plesek, *Chem. Rev.*, 1992, **92**, 269; (*d*) M. F. Hawthorne, *Current Topics in the Chemistry of Boron*, ed. G. Kabalka, The Royal Society of Chemistry, Cambridge, 1994, p. 207; (*e*) M. F. Hawthorne, *Advances in Boron Chemistry*, The Royal Society of Chemistry, Cornwall, 1997, p. 261; (*f*) F. Teixidor, R. Núñez, C. Viñas, R. Sillanpää and R. Kivekäs, *Angew. Chem., Int. Ed.*, 2000, **39**, 4290; (*g*) R. B. King, *Chem. Rev.*, 2001, **101**, 1119; (*h*) R. N. Grimes, *J. Chem. Educ.*, 2004, **81**, 657; (*i*) A. González-Campo, B. Boury, F. Teixidor and R. Núñez, *Chem. Mater.*, 2006, **18**, 4344; (*j*) K. Wade, *Nat. Chem.*, 2009, **1**, 92.

6 Lead reviews with respect to the supramolecular chemistry of icosahedral heteroboranes (*a*) P. C. Andrews, M. J. Hardie and C. L. Raston, *Coord. Chem. Rev.*, 1999, **189**, 169; (*b*) M. J. Hardie and C. L. Raston, *Chem. Commun.*, 1999, 1153; (*c*) P. C. Andrews and C. L. Raston, *J. Organomet. Chem.*, 2000, **600**, 174; (*d*) M. A. Fox and A. K. Hughes, *Coord. Chem. Rev.*, 2004, **248**, 457, and references therein; (*e*) J. Fanfrlík, M. Lepšik, D. Horinek, Z. Havlas and P. Hobza, *ChemPhysChem*, 2006, **7**, 1100.

7 See for example (*a*) L. Crăciun and R. Custelcean, *Inorg. Chem.*, 1999, **38**, 4916; (*b*) M. J. Hardie, P. D. Godfrey and C. L. Raston, *Chem.–Eur. J.*, 1999, **5**, 1828; (*c*) H. Lee, C. B. Knobler and M. F. Hawthorne, *Chem. Commun.*, 2000, 2485 and references therein; (*d*) E. S. Alekseyeva, A. S. Batsanov, L. A. Boyd, M. A. Fox, T. G. Hibbert, J. A. K. Howard, J. A. H. MacBride, A. Mackinnon and K. Wade, *Dalton Trans.*, 2003, 475.

8 See for example (*a*) W. Jiang, D. E. Harwell, M. D. Mortimer, C. B. Knobler and M. F. Hawthorne, *Inorg. Chem.*, 1996, **35**, 1996; (*b*) M. J. Hardie and C. L. Raston, *Eur. J. Inorg. Chem.*, 1999, 195 and*CrystEngComm* 2001, 39, 1; (*c*) M. Nishio, *Encyclopedia of Supramolecular Chemistry*, Marcel Dekker, New York, 2004, p. 1576.

9 (*a*) E. S. Shubina, E. V. Bakhmutova, A. M. Filin, I. B. Sivaev, L. N. Teplitskaya, A. L. Chistyakov, I. V. Stankevich, V. I. Bakhmutov, V. I. Bregadze and L. M. Epstein, *J. Organomet. Chem.*, 2002, **657**, 155; (*b*) C. Viñas, A. Laromaine, F. Teixidor, H. Horàková, A. Langauf, R. Vespalec, I. Mata and E. Molins, *Dalton Trans.*, 2007, 3369; (*c*) J. Dou, F. Su, Y. Nie, D. Li and D. Wang, *Dalton Trans.*, 2008, 4152.

10 F. Di Salvo, J. G. Planas, C. Viñas, F. Teixidor, M. E. Light, M. B. Hursthouse and N. Aliaga-Alcalde, manuscript in preparation.

11 (*a*) V. Terrasson, J. G. Planas, D. Prim, C. Viñas, F. Teixidor, M. E. Light and M. B. Hursthouse, *J. Org. Chem.*, 2008, **73**, 9140; (*b*) V. Terrasson, J. G. Planas, D. Prim, F. Teixidor, C. Viñas, M. E. Light and M. B. Hursthouse, *Chem.–Eur. J.*, 2009, **15**, 12030.

12 L. I. Zakharkin, A. V. Grebennikov and A. V. Kazantsev, *Izv. Akad. Nauk SSSR, Ser. Khim.*, 1967, **9**, 2077.

13 (*a*) A. Gomez and M. F. Hawthorne, *J. Org. Chem.*, 1992, **57**, 1384; (*b*) C. Viñas, R. Benakki, F. Teixidor and J. Cassabó, *Inorg. Chem.*, 1995, **34**, 3844; (*c*) J. F. Valliant, K. J. Guenther, A. S. King, P. Morel, P. Schaffer, O. O. Sogbein and K. A. Stephenson, *Coord. Chem. Rev.*, 2002, **232**, 173.

14 A. D. Musteti, *Oxy Solvents Influence on $C_{cluster}$-Monosubstituted Derivatives of 1,2-Dicarba*-closo-*Dodecaborane with Sulphur and Chlorodiphenylphosphine*, Master thesis, 2009.

15 L. J. Todd, *Prog. Nucl. Magn. Reson. Spectrosc.*, 1979, **13**, 87.

16 A. Bacchi, M. Carcelli, T. Chiodo, G. Cantoni, C. De Filippo and S. Pipolo, *CrystEngComm*, 2009, **11**, 1433.

17 R. Sedlák, J. Fanfrlík, D. Hnyk, P. Hobza and M. Lepšík, *J. Phys. Chem. A*, 2010, **114**, 11304.

18 (*a*) M. A. Spackman and J. J. McKinnon, *CrystEngComm*, 2002, **4**, 378; (*b*) J. J. McKinnon, M. A. Spackman and A. S. Mitchell, *Acta Crystallogr., Sect. B: Struct. Sci.*, 2004, **60**, 627; (*c*) J. J. McKinnon, D. Jayatilaka and M. A. Spackman, *Chem. Commun.*, 2007, 3814; (*d*) J. J. McKinnon, F. P. A. Fabbiani and M. A. Spackman, *Cryst. Growth Des.*, 2007, **7**, 755; (*e*) M. A. Spackman and D. Jayatilaka, *CrystEngComm*, 2009, **11**, 19.

19 A. Simperler, S. W. Watt, P. A. Bonnet, W. Jones and W. D. S. Motherwell, *CrystEngComm*, 2006, **8**, 589.

20 A. Bondi, *Chem. Rev.*, 1967, **67**, 565.

21 R. J. C. Brown and R. F. C. Brown, *J. Chem. Educ.*, 2000, **77**, 724.

22 (*a*) Y. L. Slovokhotov, A. S. Batsanov and J. A. K. Howard, *Struct. Chem.*, 2007, **18**, 477; (*b*) Y. L. Slovokhotov, I. S. Neretin and J. A. K. Howard, *New J. Chem.*, 2004, **28**, 967.

23 M. J. Frisch, G. W. Trucks, H. B. Schlegel, G. E. Scuseria, M. A. Robb, J. R. Cheeseman, J. A. Montgomery, Jr, T. Vreven, K. N. Kudin, J. C. Burant, J. M. Millam, S. S. Iyengar, J. Tomasi, V. Barone, B. Mennucci, M. Cossi, G. Scalmani, N. Rega, G. A. Petersson, H. Nakatsuji, M. Hada, M. Ehara, K. Toyota, R. Fukuda, J. Hasegawa, M. Ishida, T. Nakajima, Y. Honda, O. Kitao, H. Nakai, M. Klene, X. Li, J. E. Knox, H. P. Hratchian, J. B. Cross, V. Bakken, C. Adamo, J. Jaramillo, R. Gomperts, R. E. Stratmann, O. Yazyev, J. Austin, R. Cammi, C. Pomelli, J. W. Ochterski, P. Y. Ayala, K. Morokuma, G. A. Voth, P. Salvador, J. J. Dannenberg, V. G. Zakrzewski, S. Dapprich, A. D. Daniels, M. C. Strain, O. Farkas, D. K. Malick, A. D. Rabuck, K. Raghavachari, J. B. Foresman, J. V. Ortiz, Q. Cui, A. G. Baboul, S. Clifford, J. Cioslowski, B. B. Stefanov, G. Liu, A. Liashenko, P. Piskorz, I. Komaromi, R. L. Martin, D. J. Fox, T. Keith, M. A. Al-Laham, C. Y. Peng, A. Nanayakkara, M. Challacombe, P. M. W. Gill, B. Johnson, W. Chen, M. W. Wong, C. Gonzalez, and J. A. Pople, *Gaussian 03, Revision C.02*, Gaussian, Inc., Wallingford, CT, 2004.

24 (*a*) A. D. Becke, *J. Chem. Phys.*, 1993, **98**, 5648; (*b*) C. Lee, W. Yang and R. Parr, *Phys. Rev. B*, 1988, **37**, 785.

25 R. Krishnan, J. S. Binkley, R. Seeger and J. A. Pople, *J. Chem. Phys.*, 1980, **72**, 650.

26 N. Godbout, D. R. Salahub, J. Andzelm and E. Wimmer, *Can. J. Chem.*, 1992, **70**, 560.

27 A. J. M. Duisenberg, Indexing in single-crystal diffractometry with an obstinate list of reflections, *J. Appl. Crystallogr.*, 1992, **25**, 92–96.

28 *COLLECT Data Collection Software*, Nonius B.V., 1998.

29 Z. Otwinowski and W. Minor, *Processing of X-Ray Diffraction Data Collected in Oscillation Mode, Methods in Enzymology, Volume 276: Macromolecular Crystallography, part A*, ed. C. W. Carter, Jr and R. M. Sweet, Academic Press, 1997, pp.307–326.

30 G. M. Sheldrick, *SADABS—Bruker Nonius area detector scaling and absorption correction—V2.10*.

31 G. M. Sheldrick, *SHELX97: Programs for Crystal Structure Analysis (Release 97-2)*, Institüt für Anorganische Chemie der Universität, Tammanstrasse 4, D-3400 Göttingen, Germany, 1998.

32 A. J. M. Duisenberg, L. M. J. Kroon-Batenburg and A. M. M. Schreurs, An intensity evaluation method: EVAL-14, *J. Appl. Crystallogr.*, 2003, **36**, 220–229.

